The Journal of Experimental Medicine

Protein kinase D at the Golgi controls NLRP3 inflammasome activation

Zhirong Zhang,[1,2,3,4] Gergö Meszaros,[1,2,3,4,5]* Wan-ting He,[6]* Yanfang Xu,[1,2,3,4,7,8]
Helena de Fatima Magliarelli,[1,2,3,4] Laurent Mailly,[4,9] Michael Mihlan,[1,2,3,4] Yansheng Liu,[10]
Marta Puig Gámez,[1,2,3,4] Alexander Goginashvili,[1,2,3,4] Adrien Pasquier,[1,2,3,4] Olga Bielska,[1,2,3,4]
Bénédicte Neven,[11,12] Pierre Quartier,[11,12] Rudolf Aebersold,[10,13] Thomas F. Baumert,[4,9,14]
Philippe Georgel,[4,15] Jiahuai Han,[6] and Romeo Ricci[1,2,3,4,5]

[1]Institut de Génétique et de Biologie Moléculaire et Cellulaire, Illkirch, France
[2]Centre National de la Recherche Scientifique, UMR7104, Illkirch, France
[3]Institut National de la Santé et de la Recherche Médicale, U964, Illkirch, France
[4]Université de Strasbourg, Strasbourg, France
[5]Laboratoire de Biochimie et de Biologie Moléculaire, Nouvel Hôpital Civil, Strasbourg, France
[6]State Key Laboratory of Cellular Stress Biology, Innovation Center for Cell Signaling Network, School of Life Sciences, Xiamen University, Xiamen, Fujian, China
[7]Department of Nephrology, First Affiliated Hospital, Fujian Medical University, Fuzhou, China
[8]State Key Laboratory of Kidney Diseases, National Clinical Research Center of Kidney Diseases, Chinese PLA General Hospital, Beijing, China
[9]Institut National de la Santé et de la Recherche Medicale (INSERM), U1110, Institut de Recherche sur les Maladies Virales et Hépatiques, Strasbourg, France
[10]Department of Biology, Institute of Molecular Systems Biology, Eidgenössische Technische Hochschule, Zurich, Switzerland
[11]Institut IMAGINE, Sorbonne Paris Cité, Université Paris-Descartes, Paris, France
[12]Unité d'immuno-hématologie pédiatrique, Hôpital Necker-Enfant Malades, Assistance Publique des Hôpitaux de Paris, Paris, France
[13]Faculty of Science, University of Zurich, Zurich, Switzerland
[14]Institut Hospitalo-Universitaire, Pôle Hépato-digestif, Nouvel Hôpital Civil, Strasbourg, France
[15]ImmunoRhumatologie Moléculaire, INSERM UMR_S1109, LabEx TRANSPLANTEX, Centre de Recherche d'Immunologie et d'Hématologie, Faculté de Médecine, Fédération Hospitalo-Universitaire OMICARE, Fédération de Médecine Translationnelle de Strasbourg, Strasbourg, France

The inflammasomes are multiprotein complexes sensing tissue damage and infectious agents to initiate innate immune responses. Different inflammasomes containing distinct sensor molecules exist. The NLRP3 inflammasome is unique as it detects a variety of danger signals. It has been reported that NLRP3 is recruited to mitochondria–associated endoplasmic reticulum membranes (MAMs) and is activated by MAM–derived effectors. Here, we show that in response to inflammasome activators, MAMs localize adjacent to Golgi membranes. Diacylglycerol (DAG) at the Golgi rapidly increases, recruiting protein kinase D (PKD), a key effector of DAG. Upon PKD inactivation, self–oligomerized NLRP3 is retained at MAMs adjacent to Golgi, blocking assembly of the active inflammasome. Importantly, phosphorylation of NLRP3 by PKD at the Golgi is sufficient to release NLRP3 from MAMs, resulting in assembly of the active inflammasome. Moreover, PKD inhibition prevents inflammasome auto–activation in peripheral blood mononuclear cells from patients carrying NLRP3 mutations. Hence, Golgi–mediated PKD signaling is required and sufficient for NLRP3 inflammasome activation.

INTRODUCTION

Inflammasomes are large molecular platforms that are assembled in the cytoplasm in response to pathogens and danger signals. Faithful regulation of inflammasome activity is crucial to maintain efficient host defense in complex organisms. Inflammasome activation leads to maturation and secretion of the proinflammatory cytokines IL-1β and IL-18, which initiate early inflammatory responses. Moreover, it causes a fast proinflammatory form of cell death called pyroptosis (Rathi-

nam and Fitzgerald, 2016). Uncontrolled inflammasome activation contributes to development of neurodegenerative, metabolic, and autoimmune/autoinflammatory diseases as well as cancer (Strowig et al., 2012; Broz and Dixit, 2016).

Different sensing molecules of the family of cytoplasmic pattern-recognition receptors form distinct inflammasome complexes specialized to detect specific pathogen components and/or danger signals (Lamkanfi and Dixit, 2012). The NLRP3 inflammasome is unique in the sense that it is capable of detecting a broad variety of danger signals. Activation of the NLRP3 inflammasome occurs in two steps. Priming through cytokine or pattern-recognition receptor signaling leads to

transcription and translation of NLRP3 and pro–IL-1β. Different stimuli, including ATP, toxins, and crystalline reagents, in turn trigger assembly of the inflammasome, a multimeric protein complex consisting of NLRP3, the adaptor protein apoptosis-associated speck-like protein (ASC), and pro–caspase-1. Assembly of these components leads to autoactivation of caspase-1, which cleaves pro–IL-1β and pro–IL-18 into mature cytokines (Schroder and Tschopp, 2010; Latz et al., 2013; Lamkanfi and Dixit, 2014). The cleavage of gasdermin D (GSDMD), which has been recently identified as a novel substrate of inflammatory caspases, leads to pyroptosis and secretion of IL-1β and IL-18 (He et al., 2015; Kayagaki et al., 2015; Shi et al., 2015).

Many mechanisms leading to assembly of the NLRP3 inflammasome have been proposed, but their links still need to be characterized. Among those, efflux of K^+ appears to be a crucial upstream event required to activate the NLRP3 inflammasome (Pétrilli et al., 2007). But how low intracellular K^+ induces assembly of NLRP3 is unclear. Recently, it has been shown that NEK7 acts downstream of K^+ efflux to bind NLRP3, promoting its self-oligomerization (He et al., 2016; Schmid-Burgk et al., 2016; Shi et al., 2016). Several studies also provide evidence for Ca^{2+} mobilization to be important for NLRP3 inflammasome activation (Lee et al., 2012; Murakami et al., 2012; Rossol et al., 2012). A direct implication of intracellular Ca^{2+} signaling was, however, recently debated (Muñoz-Planillo et al., 2013; Katsnelson et al., 2015). It was thus rather proposed that release of Ca^{2+} from the ER to mitochondria trigger mitochondrial Ca^{2+} overload and injury (Lee et al., 2012; Murakami et al., 2012). Damaged mitochondria in turn release several factors that activate the NLRP3 inflammasome (Nakahira et al., 2011; Shimada et al., 2012; Iyer et al., 2013). Release of Ca^{2+} from the ER is mediated through inositol-1, 4, 5-trisphosphate (InsP$_3$), a product of phospholipase C (PLC). Even though mechanisms leading to PLC activity are unknown, its involvement in NLRP3 inflammasome activation has recently been reported (Lee et al., 2012; Chae et al., 2015). Although PLC-mediated generation of InsP$_3$ and Ca^{2+} overload may trigger mitochondrial damage, the role of the other product of PLC activation, diacylglycerol (DAG), remains unexplored in this context. Importantly, NLRP3 was shown to directly bind to mitochondria-associated ER membranes (MAMs; Zhou et al., 2011; Yang et al., 2015). However, the fully active NLRP3 inflammasome is cytoplasmic, suggesting that its maturation requires additional steps.

In this study, we show that PKD signaling emanating from the Golgi is required for full maturation of the NLRP3 inflammasome. In response to NLRP3 inflammasome activators, MAMs localize adjacent to Golgi membranes. At the molecular level, enhanced DAG levels at the Golgi recruits and activates PKD, which subsequently phosphorylates NLRP3, releasing it from MAMs and resulting in assembly of the fully mature inflammasome in the cytosol.

RESULTS

MAMs localize adjacent to the Golgi, where DAG is enriched upon NLRP3 inflammasome activation

A current model suggests that signaling converging into PLC leads to generation of InsP$_3$, inducing InsP$_3$ receptor (InsP$_3$R)–mediated release of Ca^{2+} from the ER to mitochondria and mitochondrial Ca^{2+} overload and injury (Lee et al., 2012; Murakami et al., 2012). Damaged mitochondria in turn release several factors that trigger activation of the NLRP3 inflammasome (Nakahira et al., 2011; Zhou et al., 2011; Iyer et al., 2013; Subramanian et al., 2013; Wang et al., 2014; Gurung et al., 2015). We tested whether DAG, the other product of PLC activation, was involved in NLRP3 inflammasome activation. Using a reporter consisting of a GFP fused to the C1 domains of protein kinase C δ (PKCδ) that bind DAG (Codazzi et al., 2001), we monitored localized production of DAG in mouse BMDMs in response to nigericin-induced inflammasome activation. Although the reporter was mainly present in the cytosol and localized only partially to the Golgi in nonstimulated cells, its localization was almost exclusively confined to this organelle in nigericin-stimulated cells, indicating that DAG production in Golgi membranes was enhanced. Inhibition of PLC by U71322 decreased Golgi localization of the reporter in nigericin-stimulated cells (Fig. 1 A). DAG accumulation at Golgi occurred upstream of inflammasome activation, as deletion of *NLRP3* did not affect it (Fig. 1 B). Mitochondria associated with ER membranes release effectors that have been reported to mediate activation of the NLRP3 inflammasome (Nakahira et al., 2011; Zhou et al., 2011; Iyer et al., 2013; Subramanian et al., 2013; Wang et al., 2014; Gurung et al., 2015). Coimmunostaining with markers for mitochondria and Golgi revealed that mitochondria predominantly clustered around the Golgi apparatus in BMDMs treated with different NLRP3 inflammasome activators (Fig. 2 A). This observation was confirmed in THP-1 cells, a human monocyte cell line (Fig. 2 B). Mitochondrial clustering close to Golgi was not affected by deletion of *NLRP3* in BMDMs (Fig. 2 A).

Disruption of Golgi integrity with brefeldin A (BFA) markedly reduced caspase-1 cleavage, IL-1β cleavage and secretion, and the formation of ASC specks (in ∼63% of DMSO-treated and ∼15% of BFA-treated cells) upon inflammasome activation in BMDMs (Fig. 3, A–D). Activation of other inflammasomes (AIM2, NLRC4, and PYRIN inflammasome) did not evoke mitochondrial clustering around the Golgi (Fig. 2 C), suggesting that the observed organelle distribution is specific for NLRP3 inflammasome activation. These data let us to hypothesize that DAG-dependent Golgi signaling close to MAMs might be important in NLRP3 inflammasome activation.

PKD activity is required for NLRP3 inflammasome activation

One of the key effectors of DAG at the Golgi is PKD (Liljedahl et al., 2001; Baron and Malhotra, 2002). Indeed, PKD was enriched in the Golgi fraction in response to NLRP3
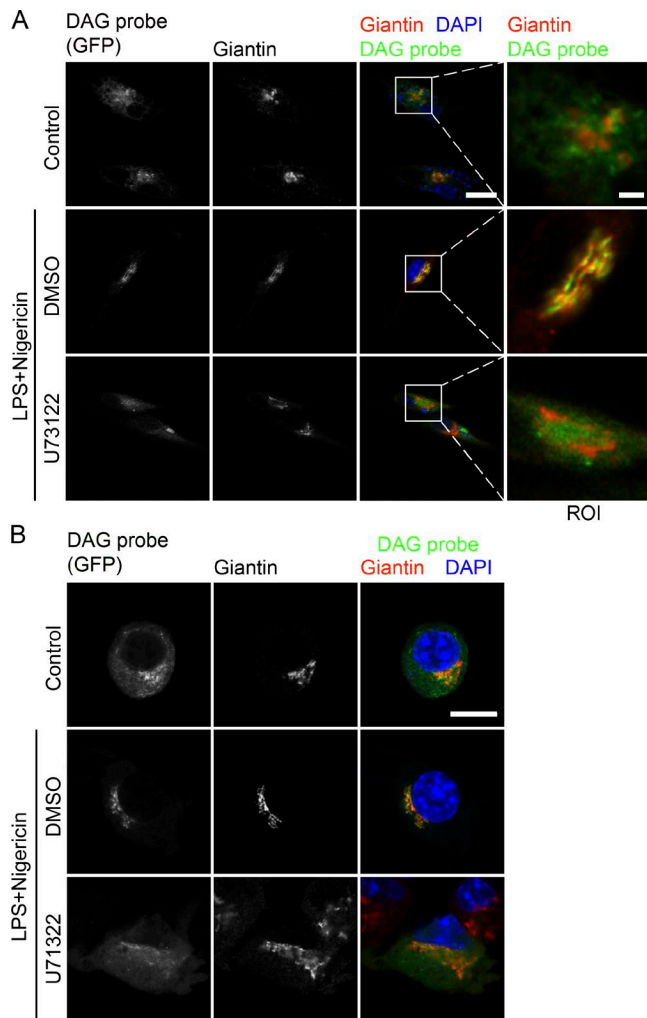
Figure 1. **Activation of NLRP3 inflammasome induces DAG enrichment in the Golgi.** (A) Confocal fluorescence imaging of LPS-primed WT BMDMs ectopically expressing a GFP-tagged DAG probe pretreated with DMSO or 10 µM U71322 for 1 h, followed by 7.5 µM nigericin stimulation for 20 min in the presence of DMSO or 10 µM U71322. Cells were immunostained using an antibody against giantin (a marker for Golgi). Nuclei were stained with DAPI. Regions of interest (ROI) are indicated by boxes. Bars: 10 µm; [region of interest (ROI)] 2 µm. (B) Confocal fluorescence imaging of LPS-primed *NLRP3*-KO BMDMs ectopically expressing a GFP-tagged DAG probe (GFP) pretreated with DMSO or 10 µM U71322 for 1 h, followed by 7.5 µM nigericin stimulation for 20 min in presence of DMSO or 10 µM U71322. Cells were immunostained with an antibody against giantin. Nuclei were stained with DAPI. Bar, 10 µm. Data shown are representative of three independent experiments.

inflammasome activation, which was not affected by PKD inhibition (Fig. S1 A). We next tested whether PKD activity is required for activation of the NLRP3 inflammasome. Strikingly, four different PKD inhibitors (CRT 0066101, Gö 6976, CID 755673, and kb NB 142–70) almost completely abolished inflammasome activity in stimulated peritoneal macrophages and/or BMDMs without affecting expression of

NLRP3, pro–caspase-1, pro–IL-1β, and ASC (Fig. 4, A and B; and Fig. S1, B and C). As previously reported (Lee et al., 2012), the InsP$_3$R antagonist 2-APB almost completely blocked inflammasome activation (Fig. 4, A and B; and Fig. S1 C). The PKC inhibitor Gö 6983, which does not inhibit PKD activity (Uesugi et al., 2012), had no such effect (Fig. 4, A and B; and Fig. S1 C). Inflammasome activation was also dramatically reduced upon PKD inhibition in human PBMCs (Fig. 4 C).

The PKD family consists of three members: PKD1, PKD2, and PKD3 (Rykx et al., 2003). To further corroborate the requirement of PKD activity in NLRP3 inflammasome activation, we generated myeloid-specific *PKD1-PKD3* double-KO (*PKD1-PKD3*$^{\Delta my}$) mice (Fig. S1 D). NLRP3 inflammasome activation in BMDMs isolated from *PKD1-PKD3*$^{\Delta my}$ mice was markedly reduced as compared with cells isolated from floxed control mice (*PKD1-PKD3*$^{fl/fl}$; Fig. 4, D–F). Inhibition was not as prominent as in PKD inhibitor–treated cells, most likely because of the remaining PKD2 activity. Indeed, additional pharmacologic inhibition of PKD (Fig. 4, D–F) or siRNA-mediated knockdown of *PKD2* (Fig. 4 G) abolished inflammasome activity in KO cells. The development of the myeloid lineage was not affected in *PKD1-PKD3*$^{\Delta my}$ mice (Fig. S1, E and F). Priming and release of other NF-κB–dependent cytokines were not impaired in BMDMs from *PKD1-PKD3*$^{\Delta my}$ mice (Fig. S1, D, G, and H). To further corroborate that remaining PKD2 activity in KO cells was indeed responsible for residual inflammasome activity, we generated Raw-ASC macrophages lacking *PKD1*, *PKD2*, and *PKD3* (Fig. S1 I). Strikingly, caspase-1 cleavage and secretion in response to nigericin was completely abolished in these cells as compared with WT cells (Fig. 4 I). Inhibition was comparable to the one seen in *NLRP3*-KO cells. As expected, caspase-1 was undetectable in *Caspase-1*–KO cells. In line with previous studies (He et al., 2015; Kayagaki et al., 2015; Shi et al., 2015), caspase-1 cleavage was partially maintained, whereas its secretion was abolished in *GSDMD*-KO cells (Fig. 4 I).

Flagellin-induced NLRC4-, dsDNA-induced AIM2-, and cytotoxin TcdB-induced PYRIN inflammasome activation was not affected in BMDMs upon PKD inhibition. Inhibition of PKD upon NLRC4 inflammasome activation did not change autocleavage of caspase-1 (Fig. S2 A). The same was true for AIM2 and PYRIN inflammasome activation, of which formation of ASC specks was also unchanged (Fig. S2 B).

Several studies have shown that gram-negative bacteria (*Escherichia coli*) and gram-positive bacteria (*Staphylococcus aureus*) activated the NRLP3 inflammasome (Mariathasan et al., 2006; Sander et al., 2011). In line with these studies, activation of NLRP3 inflammasome-dependent cleavage of caspase-1 in response to both *E. coli* DH5α and *S. aureus* was abolished in *NLRP3*-KO cells (Fig. 5 A). In comparison with WT cells, the cleavage of caspase-1 was markedly decreased in *PKD1-PKD3*$^{\Delta my}$ cells (Fig. 5 A).

To corroborate the role of PKD in NLRP3 inflammasome activation in vivo, we first treated mice with LPS by i.p. injection in the absence or presence of PKD inhi-
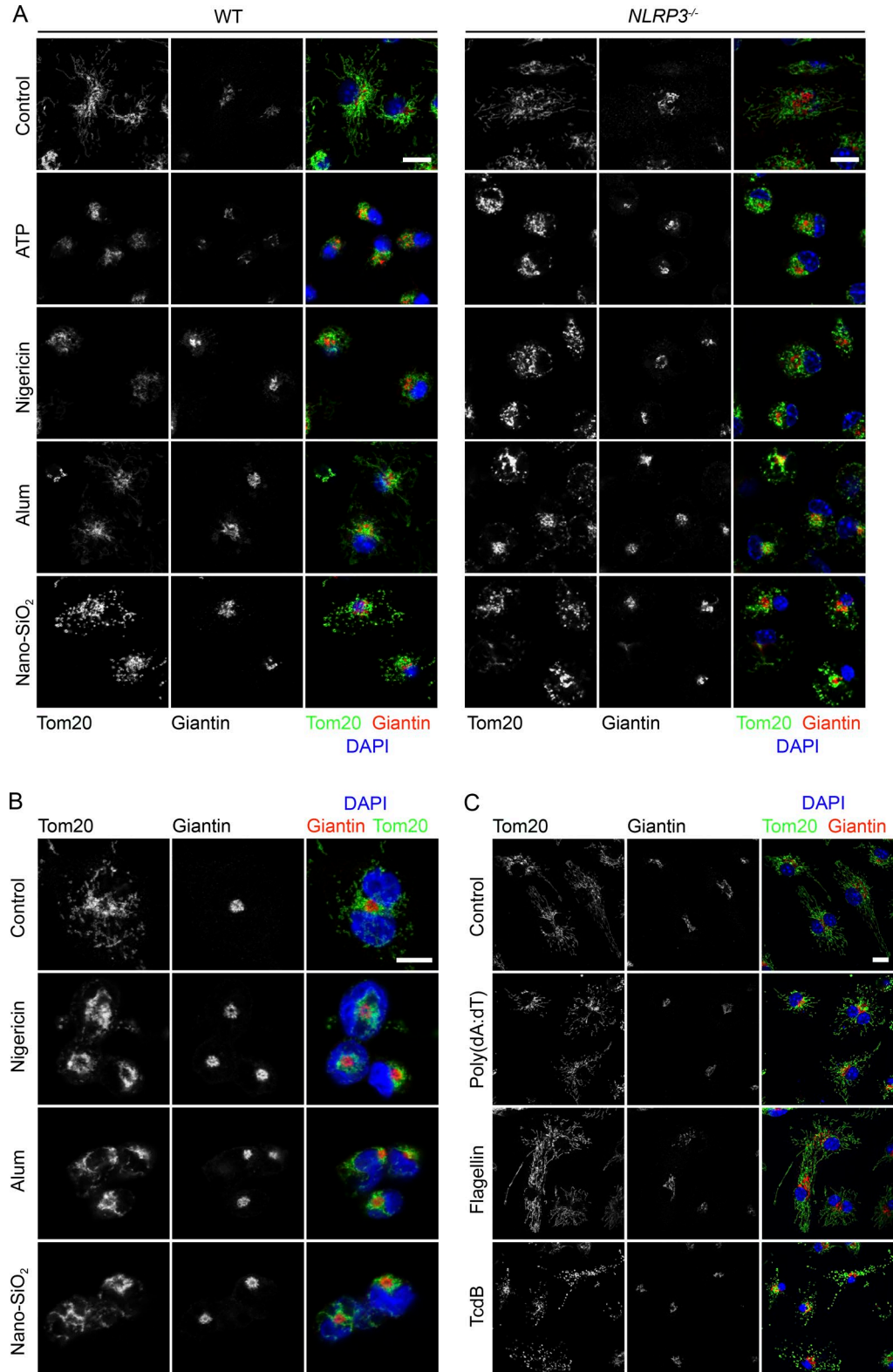
Figure 2. **Activation of NLRP3 inflammasome induces mitochondrial clustering around the Golgi.** (A) Confocal fluorescence imaging of LPS-primed WT and *NLRP3*-KO BMDMs treated or not with 5 mM ATP or 15 µM nigericin for 20 min or with 500 µg/ml alum or 125 µg/ml nano-SiO₂ for 6 h. Cells were coimmunostained using antibodies against Tom20 (a marker for mitochondria) and giantin. Nuclei were stained with DAPI. Bars, 10 µm. (B) Confocal fluorescence imaging of PMA-differentiated THP-1 cells treated or not with 15 µM nigericin for 20 min, 500 µg/ml alum, or 125 µg/ml nano-SiO₂ for 6 h.

bition. LPS injection increased the serum IL-1β level in DMSO-treated control mice (Fig. 5 B), whereas serum IL-1β was almost not detectable in *NLRP3*-KO mice (Fig. 5 B). In comparison with DMSO-treated control mice, CRT 0066101–treated mice showed dramatically reduced serum IL-1β levels (Fig. 5 B). We next addressed PKD-dependent phenotypic outcomes in mice during a bacterial challenge. Inhibition of PKD in mice subjected to i.p. injections of *S. aureus* led to a significantly enhanced mortality as compared with infected DMSO-treated control mice (Fig. 5 C). Accordingly, higher mortality was accompanied with a reduced body temperature (Fig. 5 D) as well as an increased bacterial load (Fig. 5, E and F). Similarly, *PKD1-PKD3^{Δmy}* mice showed accelerated mortality (Fig. 5 G) and lower body temperature (Fig. 5 H) as compared with *PKD1-PKD3^{fl/fl}* control mice. Our data are thus in line with previous findings in *ASC*- and *IL-1β*–deficient mice (Miller et al., 2007), supporting that PKD-mediated NLRP3-dependent IL-1 β release is an important response for efficient clearance of *S. aureus*.

Taking all together, these data thus corroborate an important role of PKD signaling in mediating NLRP3 inflammasome activity.

PKD acts downstream of mitochondrial damage and is required for the recruitment of ASC to NLRP3

Numerous studies suggest that mitochondrial damage is important for the activation of the NLRP3 inflammasome (Nakahira et al., 2011; Zhou et al., 2011; Iyer et al., 2013; Subramanian et al., 2013; Gurung et al., 2015). We thus tested whether PKD activity controls mitochondrial function in response to NLRP3 inflammasome activation. Oxygen consumption rates (OCRs) were dramatically lower in nigericin-stimulated cells (Fig. S3 B) than in control-treated cells. In line with a previous study (Shimada et al., 2012), nigericin-treated cells did not respond to oligomycin, FCCP, and rotenone/antimycin, whereas control-treated cells responded as expected. Importantly, PKD inhibition did not prevent nigericin-induced mitochondrial damage (Fig. S3 B), indicating that improved mitochondrial function did not account for NLRP3 inflammasome inactivity upon PKD inhibition. This was confirmed in *NLRP3*-null cells (Fig. S3, A and B), indicating that mitochondrial injury occurs upstream of PKD-mediated NLRP3 inflammasome activation. Moreover, PKD inhibition did not affect mitochondrial clustering close to the Golgi in response to nigericin stimulation (Fig. S3 C). Interestingly, 2-APB prevented mitochondrial clustering close to Golgi (Fig. S3 C), suggesting that InsP_3–mediated signaling is required for mitochondrial clustering.

We next asked whether PKD activity was important for recruitment of ASC to NLRP3. Strikingly, almost no ASC specks were found in stimulated BMDMs and THP-1 cells upon PKD inhibition, whereas they were present in ∼17% and ∼31% of respective control cells (Fig. 6, A–D). Immunoblotting with cross-linked pelleted protein extracts corroborated reduced oligomerization of ASC upon PKD inhibition (Fig. 6 E). Stimulation of BMDMs from *PKD1-PKD3^{fl/fl}* mice with ATP and nigericin resulted in ASC speck formation in ∼23% and ∼55% of cells, respectively. ASC speck formation was reduced in cells derived from *PKD1-PKD3^{Δmy}* mice to ∼8% and ∼25%, respectively (Fig. 6 F). Overall, these data indicate that PKD activity downstream of mitochondrial clustering and injury is required for the recruitment of ASC to NLRP3.

PKD inactivation results in retention of NLRP3 at MAMs adjacent to Golgi

NLRP3 was shown to directly bind to MAMs (Zhou et al., 2011; Yang et al., 2015). We thus further tested whether PKD deficiency affected subcellular localization of NLRP3. NLRP3 was found in small foci that predominantly colocalized with ASC specks in ∼35% of nigericin-stimulated THP-1 cells. In contrast, NLRP3 staining was more diffuse forming larger disc-like structures in ∼70% of THP-1 cells upon PKD inhibition (Fig. 7, A and B). *NLRP3*-KO cells did not show any visible signal of NLRP3 immunostaining (Fig. 7 A). Conventional confocal microscopy revealed partial colocalization of NLRP3 with the Golgi marker giantin in PKD-inhibited cells (Fig. 7 C). 3D-SIM superresolution microscopy revealed that there was very little colocalization with giantin, indicating that NLRP3 was very close to but did not directly bind to Golgi membranes (Fig. 7 D). We thus asked whether NLRP3 was retained at MAMs close to Golgi membranes. Indeed, biochemical fractionation demonstrated increased enrichment of NLRP3 at MAMs upon PKD inhibition (Fig. 7 E). Consistent with findings in THP-1 cells, in stimulated PKD-inhibited BMDMs, NLRP3 was found in bright foci that were slightly bigger as compared with those in control-treated cells. Most NLRP3 localized to the Golgi region upon PKD inhibition, whereas it predominantly localized to the cytoplasm in control-treated cells (Fig. S2, C and D). Consistent results were observed in stimulated BMDMs isolated from control and *PKD1-PKD3^{Δmy}* mice (Fig. S2, E and F). Altogether, these data suggest that PKD activity is required to release NLRP3 from MAMs, allowing for ASC recruitment and inflammasome activation.

PKD phosphorylates NLRP3 at Ser293 to release it from MAMs

We next tested whether PKD at the Golgi interacts and phosphorylates NLRP3 to release it from MAMs. Ectopically

---

Cells were coimmunostained with anti-Tom20 and anti-giantin antibodies. Nuclei were stained with DAPI. Bar, 10 µm. (C) Confocal fluorescence imaging of LPS-primed BMDMs treated or not with 1 µg/ml poly(dA:dT) for 4 h, 0.5 µg/ml flagellin for 4 h, or 0.1 nM Tcd B for 2 h. Cells were coimmunostained using antibodies against Tom20 and giantin. Nuclei were stained with DAPI. Bar, 10 µm. Data shown are representative of three independent experiments.
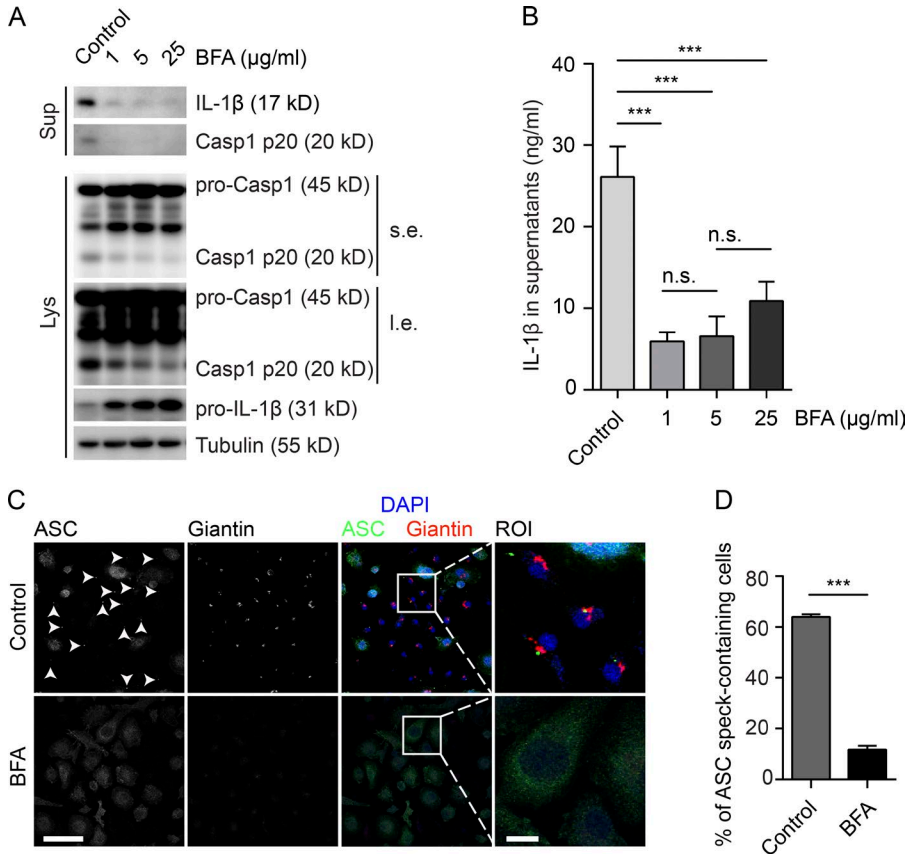
Figure 3. **Disruption of Golgi integrity blocks the NLRP3 inflammasome activation.** (A) Immunoblotting of culture supernatants (Sup) and lysates (Lys) from LPS-primed BMDMs pretreated with ethanol (control) or 1 µg/ml, 5 µg/ml, or 25 µg/ml BFA for 1 h, followed by 7.5 µM nigericin treatment for 40 min in the presence of ethanol or BFA at the indicated concentration. Antibodies against caspase-1 (recognizing both cleaved [p20] and uncleaved protein) and IL-1β (recognizing both cleaved and uncleaved protein) were used. Tubulin was used as a loading control. (B) ELISA measurements of IL-1β in culture supernatants from LPS-primed BMDMs treated as in A. The values are expressed as means ± SEM. ***, P < 0.001 (t test); n.s., not significant. (C) Confocal fluorescence imaging of LPS-primed BMDMs pretreated with ethanol or 5 µg/ml BFA for 1 h, followed by 7.5 µM nigericin treatment for 40 min in the presence of ethanol or 5 µg/ml BFA. Cells were coimmunostained with antibodies against ASC and giantin. Nuclei were stained with DAPI. Bars: 10 µm; (ROI) 2 µm. Arrowheads indicate the ASC foci. (D) Quantification of cells containing ASC foci shown in C. ***, P < 0.001 (t test). Data shown are representative of three independent experiments.

expressed PKD1 coimmunoprecipitated with ectopically expressed NLRP3 and vice versa (Fig. 8 A). Immunoblotting using a PKD substrate phospho-motif antibody revealed phosphorylation of ectopically expressed mouse NLRP3 in cells coexpressing constitutively active PKD1 (PKD1ca; Fig. 8 B). Expression of NLRP3 lacking the pyrin domain, the nucleotide-binding domain (NBD) or the leucine-rich repeat domain, respectively, revealed that phosphorylation occurred in the NBD (Figs. 8 B and S4 A). Expression of truncated and mutated NLRP3 identified phosphorylation of NLRP3 in the NBD at serine 293 (Ser293; Figs. 8 C and S4 A). Phosphorylation at Ser293 of ectopically expressed NLRP3 was confirmed by mass spectrometry (Fig. S4, B and C). This site is highly conserved among different species corresponding to Ser295 in human NLRP3 (Fig. S4 D). We next generated a phospho–Ser293–specific rabbit polyclonal antibody. Using this antibody, phosphorylation of ectopically expressed NLRP3 was detected in cells expressing WT PKD1. Expression of PKD1ca markedly enhanced phosphorylation of WT, but not S293A mutant, NLRP3 (Fig. 8 D). Other kinases (Gross et al., 2009; Chuang et al., 2011; Lu et al., 2012; Martin et al., 2014; Ito et al., 2015) that have been implicated in NLRP3 inflammasome regulation did not induce phosphorylation of NLRP3 at Ser293 (Fig. S4 E). We next aimed at corroborating phosphorylation of endogenous NLRP3. Activation of NLRP3 inflammasome by ATP and

nigericin induced phosphorylation of NLRP3 at Ser293 (Fig. 8 E). Moreover, NLRP3 foci in nigericin-stimulated THP-1 cells and ATP-stimulated BMDMs colocalized with signals specific for phospho–NLRP3 (Ser293), whereas there were no phospho–NLRP3 foci detectable in PKD-inhibited cells (Figs. 8 F and S5 A). Loss of phosphorylation of endogenous NLRP3 was confirmed in Raw-ASC macrophages lacking *PKD1*, *PKD2*, and *PKD3* (Fig. S5 B). Hence, these data indicate that PKD phosphorylates NLRP3 at Ser293. We next asked whether PKD-mediated phosphorylation controls the activation of the NLRP3 inflammasome. To this end, we reconstituted *NLRP3*-deficient THP-1 cells with WT–, nonphospho (S293A)–, and phospho-mimicking (S293E) *NLRP3*. Reconstitution with WT *NLRP3* partially restored NLRP3 inflammasome activity, as indicated by cleavage and secretion of caspase-1 and IL-1β. In comparison, the capacity of S293A NLRP3 to restore inflammasome activity was markedly lower (Fig. 8, G and H). Reconstituted WT NLRP3 formed foci in ~13% of cells, whereas S293A NLRP3 formed foci only in ~5% of cells. Importantly, S293A NLRP3 was retained in the Golgi region in ~17% cells (Fig. 8, I and J), in line with retention of endogenous WT NLRP3 at MAMs close to the Golgi in cells subjected to PKD inhibition. Together with our finding that phosphorylated NLRP3 can be found in the mature inflammasome, our data strongly suggest that PKD-mediated phosphoryla-

Figure 4. **Deficiency of PKD specifically blocks the activation of the NLRP3 inflammasome.** (A) Immunoblotting of culture supernatants (Sup) and lysates (Lys) from LPS-primed BMDMs pretreated with DMSO, 5 µM Gö 6983, 10 µM CRT 0066101, 5 µM Gö 6976, 30 µM CID 755673, or 50 µM 2-APB for 1 h, followed by ATP treatment for 40 min in the presence of DMSO or indicated inhibitors. l.e., long exposure; s.e., short exposure. (B) ELISA measurements

tion of NLRP3 releases NLRP3 from MAMs, allowing for inflammasome maturation.

It has been demonstrated that binding of NLRP3 to MAMs is crucial for its activation (Zhou et al., 2011; Subramanian et al., 2013). Constitutive phosphorylation of NLRP3 is thus expected to prevent its binding to MAMs and thus inflammasome activation. Indeed, expression of S293E NLRP3 did not restore inflammasome activity in *NLRP3*-deficient THP-1 cells (Fig. 8, G and H). Moreover, S293E NLRP3 did not form any foci localizing diffusely throughout the cytoplasm, which is in line with its inability to bind to MAMs (Fig. 8, I and J).

Our data are thus consistent with a model in which local and timely phosphorylation of membrane-bound NLRP3 by PKD results in its release and cytoplasmic assembly of the fully active inflammasome.

PKD activity at Golgi is sufficient to activate the NLRP3 inflammasome

As shown in Fig. 1, DAG production was enhanced at the Golgi to recruit PKD to this organelle upon NLRP3 inflammasome activation. Hence, PKD activity at the Golgi is expected to be sufficient to phosphorylate NLRP3 and to activate the NLRP3 inflammasome. Indeed, expression of WT, but not kinase-dead, PKD1 induced NLRP3 inflammasome-dependent activation of caspase-1 and secretion of IL-1β without stimulation (Fig. 9 A). Consistently, expression of PKD1 dramatically enhanced the activation of caspase-1 and secretion of IL-1β upon nigericin treatment. Importantly, this effect was abolished by CRT 0066101 treatment, corroborating the importance of PKD activity for NLRP3 inflammasome activation in inhibitor experiments (Fig. 9 B). Strikingly, expression of GRIP tagged-PKD1, localization of which was restricted to the Golgi, but not of PKD lacking the DAG-binding domain, was sufficient to phosphorylate NLRP3 and to activate the NLRP3 inflammasome (Fig. 9, C and D). These data thus suggest that PKD activity at the Golgi is sufficient to activate the NLRP3 inflammasome.

PKD inhibition blocks the activity of the NLRP3 inflammasome in cells from patients with autoactivatory mutations in NLRP3

Patients with cryopyrin-associated periodic syndrome (CAPS) suffer from autoinflammatory events caused by mutations in *NLRP3* resulting in its auto-oligomerization and uncontrolled NLRP3 inflammasome activation (Aksentijevich et al., 2007; Brydges et al., 2009; Nakamura et al., 2012). We next determined whether autoactivation of mutated NLRP3 inflammasome depends on PKD activity. PKD inhibition of LPS-stimulated PBMCs isolated from patients carrying the mutations T436N or R260W in the *NLRP3* gene resulted in a strong reduction of caspase-1 cleavage and IL-1β secretion as compared with control-treated cells (Fig. 10, A and B). T436N NLRP3 was stuck in disc-like structures at the Golgi upon PKD inhibition (Fig. 10 C). These mutations result in spontaneous self-oligomerization of the NLRP3 protein (Baroja-Mazo et al., 2014). These data thus corroborate that PKD inhibition is sufficient to block inflammasome activity in cells of these patients. They also indicate that PKD acts downstream of NLRP3 self-oligomerization. Indeed, a native page as well as a gel filtration assay revealed that PKD inhibition did not affect self-oligomerization of NLRP3 (Fig. S5, C and D). Given the fact that NLRP3 was retained at MAMs upon PKD inhibition, it is expected that NLRP3 at MAMs is self-oligomerized before its phosphorylation. Accordingly, oligomerization of reconstituted S293E NLRP3 was abolished, whereas oligomerization of reconstituted S293A and WT NLRP3 were unaffected in stimulated THP-1 cells (Fig. S5 E).

Altogether, we propose a model in which MAMs localize close to the Golgi in response to NLRP3 inflammasome activation. This allows for PKD-induced phosphorylation of self-oligomerized NLRP3, its release from MAMs, and assembly of the cytosolic mature inflammasome (Fig. 10 D).

DISCUSSION

In this study, we unveiled the spatial and temporal organization of NRLP3 inflammasome activation. PKD-mediated

---

of IL-1β in culture supernatants from LPS-primed BMDMs treated as in A. The values are expressed as means ± SEM. p-values were calculated between ATP alone–treated group and ATP plus inhibitor–treated group. ***, P < 0.001 (*t* test); N.D., not detected; n.s., not significant. (C) Immunoblotting of culture supernatants (Sup) and lysates (Lys) from LPS-primed PBMCs pretreated with DMSO or 10 µM CRT 0066101 for 1 h, followed by treatment with 5 mM ATP for 40 min, 15 µM nigericin for 40 min, 250 or 500 µg/ml alum for 6 h, or 125 or 250 µg/ml nano-SiO₂ for 6 h in the presence of DMSO or 10 µM CRT 0066101. (D–F) Immunoblotting of culture supernatants (Sup) and lysates (Lys) from BMDMs isolated from *LysM-Cre*–negative floxed *PKD1-PKD3* (*PKD1-PKD3^{fl/fl}*) control mice and *LysM-Cre*–positive myeloid-specific *PKD1-PKD3* double-KO (*PKD1-PKD3^{Δmy}*) mice. Cells were primed with LPS for 4 h. After pretreatment with DMSO or CRT 0066101 for 1 h, cells were stimulated with ATP for 40 min (D), alum (E), or nano-SiO₂ (F) as indicated for 6 h in the presence of DMSO or 10 µM CRT 0066101. (G) Immunoblotting of culture supernatants (Sup) and lysates (Lys) from BMDMs isolated from *PKD1-PKD3^{fl/fl}* control mice and *PKD1-PKD3^{Δmy}* mice. Cells were transfected with control siRNA (siControl) or siRNA against PKD2 (siPKD2) as indicated for 36 h. After LPS priming for 4 h, cells were treated or not with 5 mM ATP or 7.5 µM nigericin for 40 min. (H) Quantitative PCR analysis of BMDMs isolated from *PKD1-PKD3^{fl/fl}* control mice and *PKD1-PKD3^{Δmy}* mice were transfected with control siRNA (siControl) or siRNA against PKD2 (siPKD2) as indicated for 36 h. The level of *PKD2* mRNA relative to *Hprt* mRNA was analyzed by quantitative PCR. The values are expressed as means ± SEM. **, P < 0.01 (*t* test). (I) Immunoblotting of culture supernatants (Sup) and lysates together with culture supernatants (Lys + Sup) from Raw-ASC WT, *Caspase-1*–KO (*Casp1* ko), *NLRP3*-KO (*NLRP3* ko), *GSD MD*-KO (*GSDMD* ko), and *PKD1|PKD2|PKD3* triple-KO (*PKD1/2/3* ko) cells. LPS-primed cells were treated with or without 10 µM nigericin for 1 h. Asterisk (*) represents unspecific bands. Data shown are representative of at least three independent experiments.
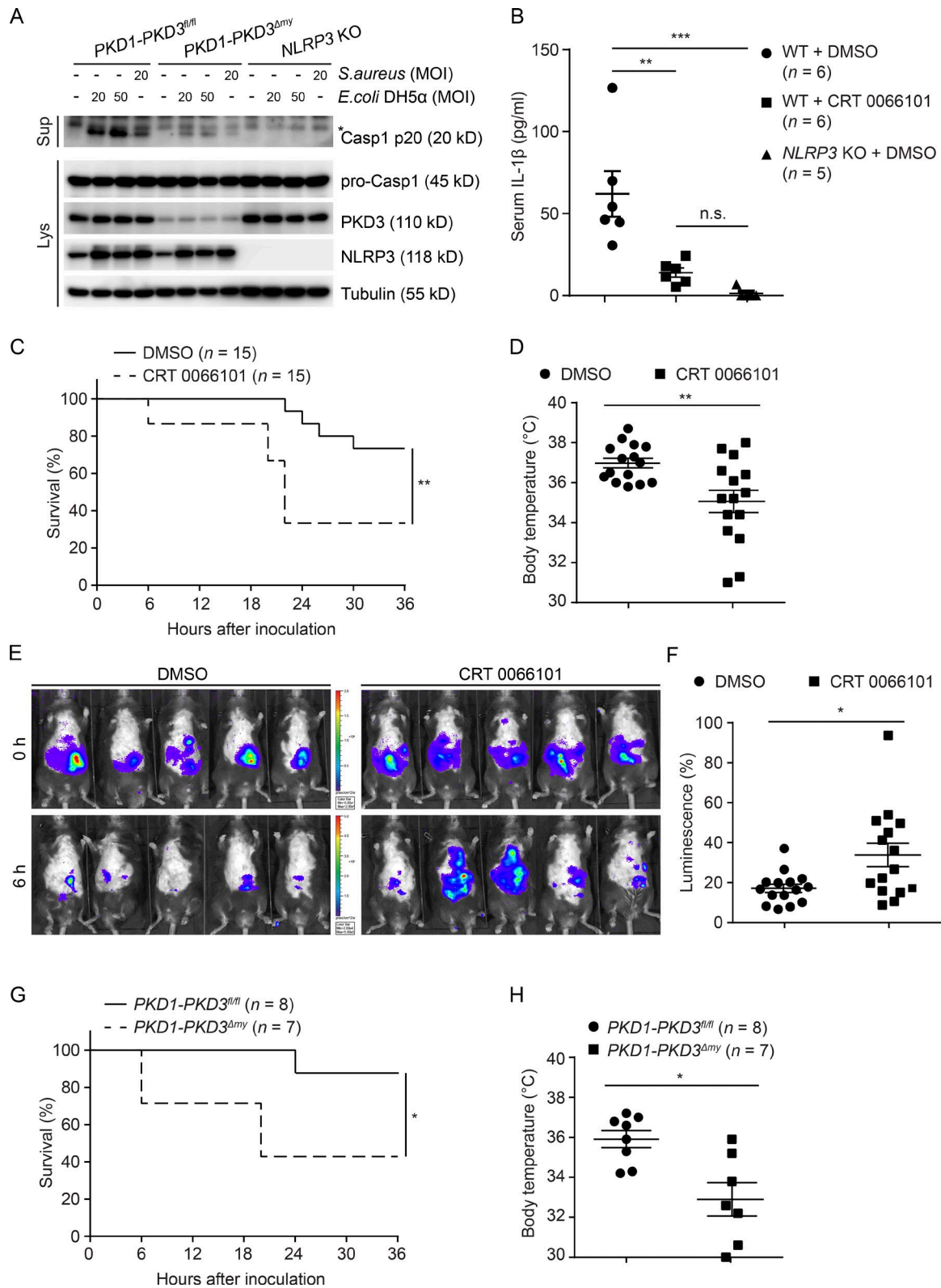
Figure 5. **PKD activity is required for NLRP3 inflammasome activation in vivo.** (A) Immunoblotting of culture supernatants (Sup) and lysates (Lys) from BMDMs isolated from *PKD1-PKD3^fl/fl* control mice, *PKD1-PKD3^Δmy* mice, and *NLRP3*-KO mice. LPS-primed cells were infected with *E. coli* DH5α or *S. aureus* at indicated multiplicity of infection (MOI) for 3 h. (B) ELISA analysis of serum IL-1β from LPS-injected mice. Mice were intraperitoneally pretreated with

signaling emanating from the Golgi close to MAMs leads to phosphorylation of NLRP3 releasing it from MAMs, a necessary step to allow for assembly of the mature NLRP3 inflammasome in the cytoplasm (Fig. 10 D).

We identified the Golgi as an important element controlling the activation of the NLRP3 inflammasome in macrophages. The importance of Golgi function is reflected by our observation that mitochondria cluster close to Golgi membranes upon inflammasome activation (Fig. 2), and that disruption of Golgi integrity blocks the activation of NLRP3 inflammasome (Fig. 3). In particular, disruption of Golgi by BFA blocked the activation of NLRP3 inflammasome and secretion of IL-1β. Rubartelli et al. (1990) showed that IL-1β was secreted via a BFA-insensitive pathway in LPS-activated monocytes. In this study, the release of IL-1β was tested in response to LPS stimulation only. Importantly, other studies have clearly demonstrated that ultrapure LPS could not trigger IL-1β release (Martinon et al., 2004, 2006). Thus, a plausible explanation is that the release of IL-1β triggered by LPS in this study was induced through activation of other inflammasomes by contaminants. Given the fact that PKD activity is not important in the activation of other inflammasomes, their readouts were most likely independent of Golgi-derived signaling. A more recent study by Menu et al. (2012) showed that ER stress was sufficient to activate the NLRP3 inflammasome in LPS-primed macrophages without inflammasome stimulators. Different compounds, including BFA, were used to promote ER stress through different mechanisms. ER stress induced by tunicamycin and thapsigargin, but not BFA, was sufficient to trigger NLRP3 inflammasome activity in LPS-primed BMDMs. This is in line with our study demonstrating that BFA, despite its effects on ER stress, blocks the activation of NLRP3 inflammasome by disrupting Golgi integrity.

The importance of Golgi function is further substantiated in our study at the molecular level. In fact, the second messenger, DAG, increased in Golgi membranes (Fig. 1), triggering local activity of the effector kinase PKD that is necessary to activate the NLRP3 inflammasome (Figs. 4 and 5). Importantly, forced targeting of PKD activity to the Golgi is sufficient to activate the NLRP3 inflammasome (Fig. 9). Finally, PKD inhibition resulted in retention of NLRP3 at

MAMs close to Golgi membranes (Fig. 7), corroborating propagation of signals from the Golgi to MAMs.

Of note, PKD is a stress kinase that senses effectors of injured mitochondria (Storz et al., 2005). Hence, in addition to DAG enrichment in the Golgi, clustering of injured mitochondria close to the Golgi may boost PKD activation, leading to phosphorylation of NLRP3 and its release from MAMs. Conversely, local exposure of NLRP3 with mitochondrial effectors may also contribute to inflammasome activation. It is likely that other molecular events occur at the interface of Golgi and MAMs that contribute to NLRP3 inflammasome activation. In particular, the identified organelle interplay might also be crucial to couple activation of NLRP3 inflammasome to IL-1β secretion. In fact, signal propagation from the Golgi to the ER mediates formation of secretory autophagosomes that have been implicated in nonconventional secretion of IL-1β (Ponpuak et al., 2015). Thus, our discovery will open a whole new avenue of interesting future research.

The importance of binding of NLRP3 to MAMs, even though it has been evidenced in the literature (Zhou et al., 2011; Yang et al., 2015), has been challenged, because the mature NLRP3 inflammasome resides in the cytosol. In fact, our study integrates both observations into one coherent model highlighting the importance of the highly dynamic spatial arrangement of intracellular organelles and localization of NLRP3. Membrane binding of NLRP3 is dependent on the N-terminal sequence of its pyrin domain (Subramanian et al., 2013). The pyrin domain is essential for NLRP3 to bind ASC (Dowds et al., 2003; Agostini et al., 2004). Thus, exposure of the pyrin domain might be essential for further maturation of the NLRP3 inflammasome. Importantly, the study by Zhou et al. (2011) demonstrated that both NLRP3 and ASC were found in MAM fractions, potentially indicating that interaction already occurred in the MAM compartment. However, this study also showed that most ASC was cytoplasmic under both nonstimulating and stimulating conditions. We thus propose that NLRP3, without or with ASC, might be released from MAMs to recruit ASC or more ASC in the cytoplasm, forming the mature inflammasome. The detailed mechanisms of phosphorylation-mediated release of NLRP3 from MAMs will be an important subject of future research. Even though speculative, phosphorylation in the NBD may change con-

---

DMSO or 10 mg/kg CRT 0066101 as indicated for 1 h, followed by intraperitoneal injection of 20 mg/kg LPS. Blood were collected at 2 h after LPS injection. The values are expressed as means ± SEM. **, P < 0.01; ***, P < 0.001; n.s., not significant (Mann–Whitney test). (C) The survival curve of *S. aureus*–infected mice. WT mice were intraperitoneally pretreated with DMSO (*n* = 15) or 10 mg/kg CRT 0066101 (*n* = 15) for 1 h, followed by intraperitoneal infection of *S. aureus* (7×10^8 per mouse). **, P < 0.01 (Gehan–Breslow–Wilcoxon test). (D–F) Analysis of *S. aureus*–infected mice shown in C. Body temperature (D) and bacterial load (E and F) of each mouse was measured at 6 h after infection. The bacterial loads were shown in percentage of luminescence at 0 h. The values are expressed as means ± SEM. *, P < 0.05; **, P < 0.01 (Mann–Whitney test). (G) The survival curve of *S. aureus*–infected *PKD1-PKD3^{fl/fl}* mice (*n* = 8) and *PKD1-PKD3^{Δmy}* (*n* = 7) mice. Mice were treated by i.p. infection of *S. aureus* (7×10^8 per mouse). *, P < 0.05 (Gehan–Breslow–Wilcoxon test). (H) Body temperature of mice shown in G at 6 h after infection. The values are expressed as means ± SEM. *, P < 0.05 (Mann–Whitney test). Data shown in A are the representative of three independent experiments, whereas images in D are representative of 15 mice in each group.
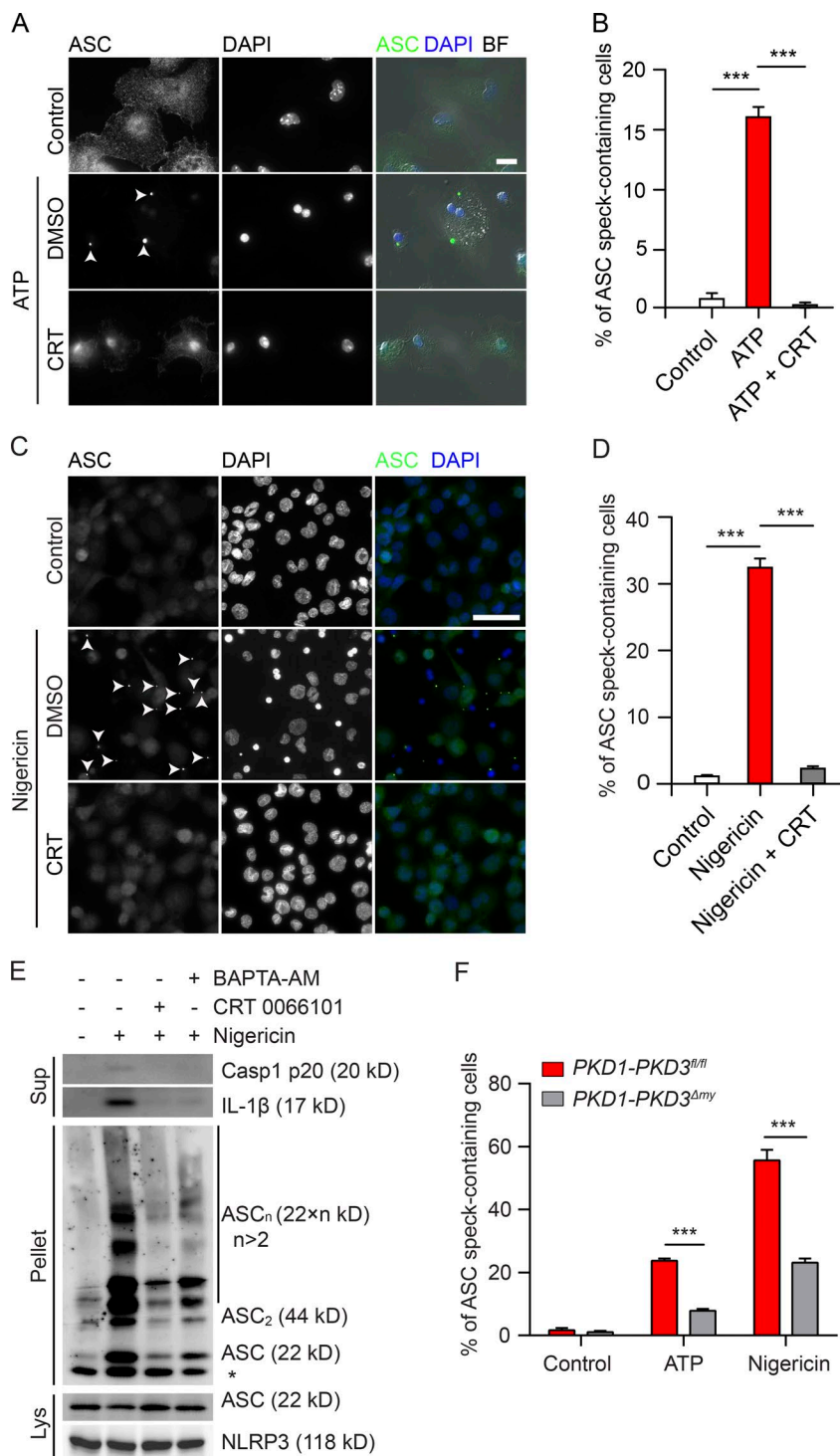
Figure 6. **Deficiency of PKD blocks recruitment of ASC to the NLRP3 inflammasome.** (A) Fluorescence imaging of LPS-primed BMDMs pretreated with DMSO or 10 µM CRT 0066101 for 1 h, followed by stimulation with 5 mM ATP in presence of DMSO or 10 µM CRT for 20 min. Cells were immunostained with an anti-ASC antibody. Nuclei were stained with DAPI. Bar, 10 µm. Merged pictures with bright-field (BF) microscopy signals are shown. Arrowheads indicate the ASC specks. (B) Quantification of ASC speck–containing BMDMs of experiments represented in A. The values are expressed as means ± SEM. ***, P < 0.001 (*t* test). (C) Fluorescence imaging of differentiated THP-1 cells pretreated with DMSO or 10 µM CRT 0066101 for 1 h, followed by stimulation with 15 µM nigericin in presence of DMSO or 10 µM CRT for 30 min. Cells were immunostained with an anti-ASC antibody. Nuclei were stained with DAPI. Bar, 50 µm. Arrowheads indicate ASC specks. (D) Quantification of ASC speck–containing THP-1 cells of experiments represented in C. The values are expressed as means ± SEM. ***, P < 0.001 (*t* test). (E) Immunoblotting of culture supernatants (Sup), lysates (Lys), and cross-linked pellets (Pellet) from differentiated THP-1 cells pretreated with DMSO, 10 µM CRT, or 25 µM BAPTA-AM for 1 h, followed by treatment with 15 µM nigericin in presence of DMSO, 10 µM CRT, or 25 µM BAPTA-AM for 40 min. (F) Quantification of ASC speck–containing LPS-primed BMDMs isolated from *PKD1-PKD3$^{fl/fl}$* and *PKD1-PKD3$^{\Delta my}$* mice. Cells were treated with 2.5 mM ATP or 7.5 µM nigericin for 20 min. The values are expressed as means ± SEM. ***, P < 0.001 (*t* test). Data shown are representative of at least three independent experiments.

formation of NLRP3 in a way it prevents membrane binding. Alternatively, chaperone-mediated release of phosphorylated NLRP3 might be important.

Recently, two studies showed that PKA negatively regulates NLRP3 inflammasome activation by phosphorylation of NLRP3 at the very same serine residue (Guo et al., 2016; Mortimer et al., 2016). In fact, inhibitory effects of this phosphorylation event is fully in line with our observation that S293E NLRP3 was unable to restore inflammasome activity in *NLRP3*-deficient THP-1 cells. However, our data also provide strong evidence for PKD-mediated phosphorylation of NLRP3 to promote inflammasome activity. Taking all these findings together, this strongly suggests that the consequences of NLRP3 phosphorylation very likely depend on where
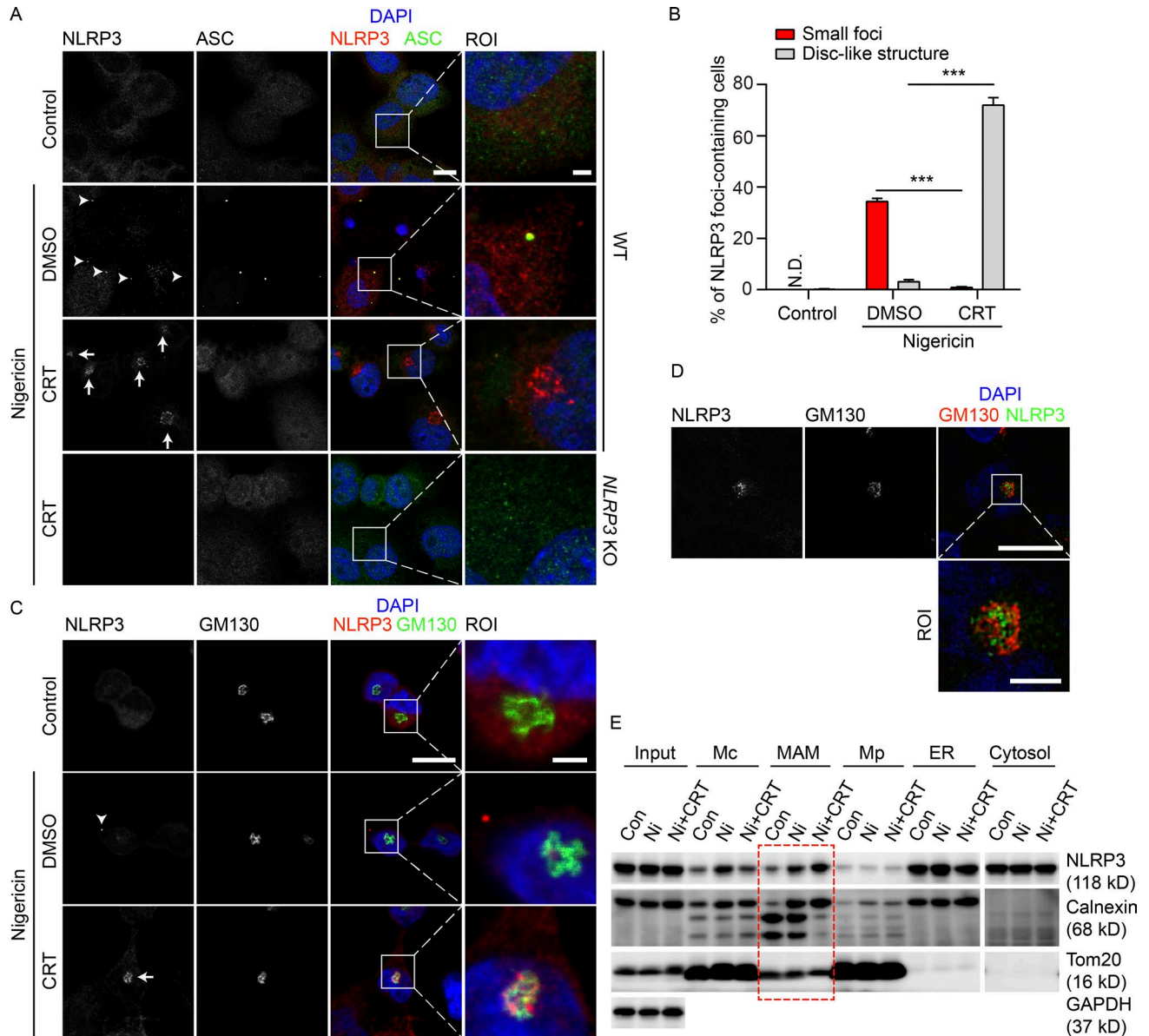
Figure 7. **PKD inhibition results in NLRP3 retention at MAMs close to Golgi.** (A) Confocal fluorescence imaging of PMA-differentiated THP-1 cells pretreated with DMSO or 10 µM CRT for 1 h, followed by stimulation with 15 µM nigericin in the presence of DMSO or CRT for 30 min. Cells were coimmunostained with anti-NLRP3 and anti-ASC antibodies. PMA-differentiated *NLRP3*-KO THP-1 cells treated with nigericin and CRT was used as a negative control for anti-NLRP3 antibody immunostaining. Nuclei were stained with DAPI. Regions of interest (ROIs) are indicated by boxes. Bars: 10 µm; (ROI) 2 µm. Arrowheads indicate small NLRP3 foci; arrows indicate NLRP3 disc-like structures. (B) Quantification of cells containing small foci or disc-like structures in experiments represented in A. The values are expressed as means ± SEM. ***, P < 0.001 (*t* test); N.D., not detected. (C) Confocal fluorescence imaging of THP-1 cells pretreated with DMSO or 10 µM CRT for 1 h, followed by stimulation with 15 µM nigericin in the presence of DMSO or CRT for 30 min. Cells were coimmunostained with antibodies against NLRP3 and GM130. Nuclei were stained with DAPI. ROIs are indicated by boxes. Bars: 10 µm; (ROI) 2 µm. The arrowhead indicates a NLRP3 small focus, whereas the arrow indicates NLRP3 distributed in a disc-like structure. (D) 3D-SIM superresolution microscopy of differentiated THP-1 cells pretreated with 10 µM CRT for 1 h, followed by stimulation with 15 µM nigericin in the presence of 10 µM CRT for 30 min. Cells were coimmunostained with antibodies against NLRP3 and GM130. Nuclei were stained with DAPI. ROIs are indicated by boxes. Bars: 10 µm; (ROI) 2 µm. (E) Immunoblotting of lysates from indicated fractionations (Mc, crude mitochondria; Mp, pure mitochondria) isolated from THP-1 cells pretreated with DMSO or 10 µM CRT for 1 h, followed by stimulation with 15 µM nigericin (Ni) in the presence of DMSO or CRT (Ni + CRT) for 30 min. Data shown are representative of at least three independent experiments.

Figure 8. **PKD phosphorylates NLRP3 at Ser293 (in mouse, Ser295 in human) to release it from MAMs.** (A) Coimmunoprecipitation of exogenous FLAG-tagged NLRP3 with HA-tagged PKD1 and vice versa in HEK293t cells. (B) Coimmunoprecipitation of exogenous FLAG-tagged WT (WT) NLRP3, NLRP3 lacking the pyrin domain (ΔPyrin), NLRP3 lacking the nucleotide-binding domain (ΔNBD), or NLRP3 lacking the leucine-rich repeats (ΔLRR) with GFP-tagged constitutively active mutant (ca) PKD1 in HEK293t cells. Asterisk (*) represents a band corresponding to autophosphorylation of GFP-tagged PKD1. (C) Coimmunoprecipitation of exogenous FLAG-tagged WT NLRP3, ΔNBD f1, ΔNBD f2, ΔNBD f3, S219A, T231A, S263;T6;9;76A (S263A; T266A; T269A; T276A), S293A, T318A, or S331;332A (S331A; S333A) NLRP3 with GFP-tagged constitutively active mutant (ca) PKD1 in HEK293t cells. Asterisk (*) represents

and when this modification occurs. In fact, phosphorylation of NLRP3 monomers by PKA may prevent its binding to MAMs, inhibiting inflammasome assembly. Local phosphorylation of self-oligomerized NLRP3 by PKD, however, releases it from MAMs, allowing for assembly of the mature inflammasome. It is possible, however, that other phosphorylation events mediated by other kinases or other posttranslational modifications downstream of PKD-mediated phosphorylation control inflammasome activation. Importantly, a very recent study showed that both nonphospho- and phospho-mimetic mutants of NRLP3 at serine 5 (Ser5) are inhibitory (Stutz et al., 2017), very similar to the observations we made with NLRP3 mutants at Ser293. Interestingly, it has been previously demonstrated that N-terminal amino acid residues from 2 to 9 are required for binding to membranes (Subramanian et al., 2013). We thus speculate that phosphorylation of Ser5, which may occur downstream of PKD-mediated phosphorylation, prevents membrane binding of NLRP3.

Other kinases, including Syk, JNK, PKR, DAPK, BTK, and IKKα, have been implicated in the activation of the NRLP3 inflammasome (Jo et al., 2016). We demonstrated that none of these kinases was capable to phosphorylate NLRP3 at Ser293 (Fig. S4 E). These data are in line with the fact that none of these kinases have been shown to phosphorylate NLRP3, nor did their inactivation result in specific phenotypes we describe in this study, in particular retention of NLRP3 in the Golgi–MAM compartment. Most recently, the kinase NEK7 has been discovered to mediate oligomerization of NLRP3, whereas its catalytic activity was shown to be redundant in this context (He et al., 2016; Shi et al., 2016). Our data are in line with these findings as PKD most likely phosphorylates NLRP3 downstream of its self-oligomerization and releases it from MAMs, allowing the assembly of mature inflammasome in cytosol (Fig. 10 D).

We also demonstrated that enrichment of DAG in Golgi membranes was PLC dependent (Fig. 1). Accordingly, PKD activity is dependent on PLC-mediated DAG production (Rozengurt et al., 2005). Our findings are fully in line with studies revealing that pharmacological inhibition of PLC blocked the activation of the NLPR3 inflammasome, whereas a PLC agonist was sufficient to activate the latter (Lee et al., 2012; Murakami et al., 2012). Activation of PLC by G protein–coupled receptor signaling at the plasma membrane was shown to be insufficient to activate the NLRP3 inflammasome (Katsnelson et al., 2015). However, the involvement of other PLC isoforms, which are activated through G protein–independent pathways (Rhee, 2001), has not been investigated. Alternatively, PLC directly at the Golgi could be critical for PKD-mediated NLRP3 inflammasome activation (Fig. 10 D). In fact, PLC-mediated generation of DAG from phosphoinositides in the Golgi complex has been reported. Both the substrates and PLC of this pathway are present in this organelle (Barker et al., 1998; Jin et al., 2001). Of note, gain-of-function mutations in phospholipase C γ2 lead to dominantly inherited autoinflammatory diseases (Yu et al., 2005; Everett et al., 2009; Abe et al., 2011; Ombrello et al., 2012; Koss et al., 2014). Patients carrying a gain of function in phospholipase C γ2 showed enhanced IL-1β production due to hyperactivation of the NLRP3 inflammasome, highlighting the importance of PLC-mediated signaling in the context of NLRP3 inflammasome activation (Zhou et al., 2012; Chae et al., 2015).

Several research teams have reported that Ca^{2+} mobilization plays an important role in NLRP3 inflammasome activation (Horng, 2014). Recently however, it has been suggested that intracellular Ca^{2+} signaling is neither necessary nor sufficient to activate the NLRP3 inflammasome (Katsnelson et al., 2015). Our model implements PLC-dependent local exchange of Ca^{2+} at MAMs that has not been monitored in the latter study. Furthermore, we found that another effect of PLC activation, DAG-mediated PKD signaling from the Golgi, was critical to release NLRP3 from MAMs allowing for full inflammasome maturation. This may explain why mobilization of Ca^{2+} by some stimuli is insufficient to activate the NLRP3 inflammasome.

Altogether, our work thus uncovered a fundamentally new organelle interplay to be at the basis of cellular innate immune responses. Finally, we propose that interference with this signaling mechanism might be a promising avenue to treat NLRP3-related inflammatory disorders, including CAPS.

a band corresponding to autophosphorylation of GFP-tagged PKD1. (D) Immunoblotting of lysates from HEK293t cells ectopically expressing FLAG-tagged WT or S293A mutant NLRP3 together with GFP-tagged WT or ca PKD1. (E) Immunoprecipitation of endogenous NLRP3 in BMDMs isolated from WT and *NLRP3*-KO mice. LPS-primed BMDMs were treated with or without 5 mM ATP or 7.5 µM nigericin as indicated for 30 min. Asterisk (*) represents an unspecific band. (F) Confocal fluorescence imaging of differentiated THP-1 cells pretreated with DMSO or 10 µM CRT 0066101 for 1 h, followed by 15 µM nigericin treatment in the presence of DMSO or 10 µM CRT 0066101 for 30 min. Cells were coimmunostained with antibodies against NLRP3 and p-NLRP3 (Ser293). Nuclei were stained with DAPI. Bar, 10 µm. The arrowhead indicates a small NLRP3 focus colocalizing with p-NLRP3 signal, whereas the arrow indicates NLRP3 distributed in a disc-like structure lacking the p-NLRP3 signal. (G) Immunoblotting of culture supernatants (Sup) and lysates (Lys) from WT and *NLRP3*-KO THP-1 cells reconstituted with empty vector (e.v.), WT, S293A, or S293E mutant *NLRP3*. PMA-differentiated cells were treated with 15 µM nigericin for 30 min. (H) ELISA measurements of IL-1β in culture supernatants from cells treated as in G. The values are expressed as means ± SEM. ***, P < 0.001 (*t* test). (I) Confocal fluorescence imaging of *NLRP3*-KO THP-1 cells reconstituted with WT, S293A, or S293E mutant *NLRP3*. Cells were coimmunostained with antibodies against NLRP3 and GM130. Nuclei were stained with DAPI. Bar, 10 µm. The arrowhead indicates a small NLRP3 focus, whereas the arrow indicates NLRP3 distributed in a disc-like structure. (J) Quantification of cells containing small foci or disc-like structures in experiments represented in I. The values are expressed as means ± SEM. **, P < 0.01; ***, P < 0.001 (*t* test). N.D., not detected. Data shown are representative of three independent experiments.

2684

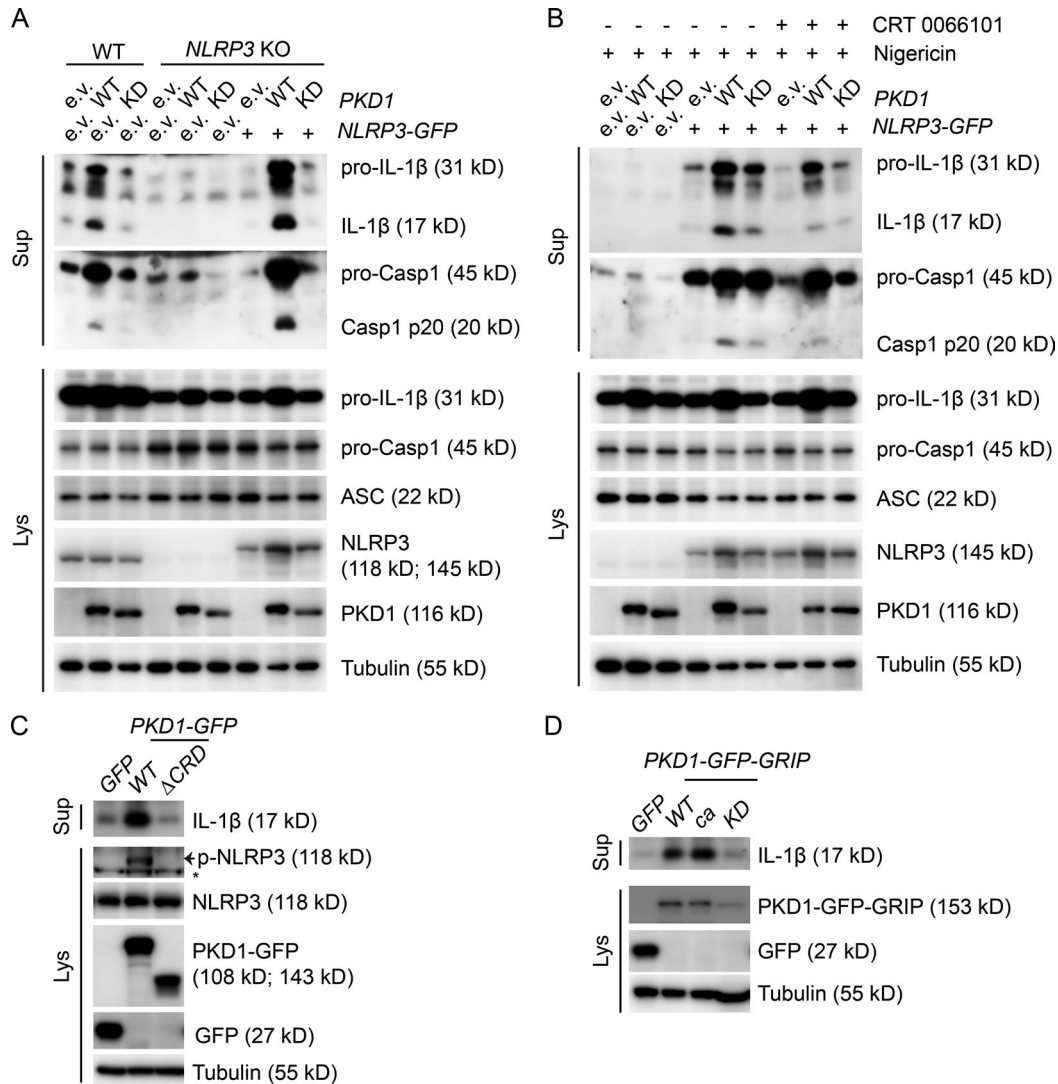Protein kinase D activates the NLRP3 inflammasome | Zhang et al.

Figure 9. **PKD activity at the Golgi is required and sufficient to activate the NLRP3 inflammasome.** (A) Immunoblotting of culture supernatants (Sup) and lysates (Lys) from THP-1 WT and *NLRP3*-KO cells infected with lentiviruses as indicated. Cells were treated with 100 nM PMA for 3 h, followed by replacement of fresh medium for 12 h. e.v., empty vector. (B) Immunoblotting of culture supernatants (Sup) and lysates (Lys) from THP-1 *NLRP3*-KO cells infected with lentiviruses as indicated. PMA-differentiated cells were pretreated with DMSO or 10 µM CRT 0066101 for 1 h, followed by 15 µM nigericin treatment in the presence of DMSO or 10 µM CRT 0066101 for 30 min. e.v., empty vector. (C and D) Immunoblotting of culture supernatants (Sup) and lysates (Lys) from stable THP-1 cell lines ectopically expressing GFP, GFP-tagged PKD1 WT, or a PKD1 mutant without the cysteine-rich domain (ΔCRD; C), GFP-GRIP-tagged WT, constitutively active (ca), or KD PKD1 (D). Cells were treated with 100 nM PMA for 3 h, followed by replacement of fresh medium for 12 h. Asterisk (*) represents an unspecific band. Data shown are representative of three independent experiments.

MATERIALS AND METHODS
Mice
NLRP3$^{-/-}$ mice on C57BL/6J background were obtained from The Jackson Laboratory. Mice with targeted alleles for *PKD1* (*PKD1*$^{fl/fl}$) were described previously (Fielitz et al., 2008). *PKD1* floxed (*PKD1*$^{fl/fl}$) mice were provided by R. Bassel-Duby and E.N. Olson (University of Texas Southwestern, Dallas, TX). Generation of *PKD3* floxed mice have been previously described (Zhang et al., 2016). We crossed *PKD1*$^{fl/fl}$

mice and *PKD3*$^{fl/fl}$ mice on C57BL/6J background with *Lys M-Cre* mice to obtain myeloid-specific *PKD1-PKD3* double-KO mice. C57BL/6J WT mice were ordered from Charles River Laboratories. Mice were housed under specific pathogen–free conditions. All animal experimentation was approved by the Direction des Services Vétérinaires du Bas-Rhin, France, except that bacteria infection experiments were approved by Comité Régional d'Ethique en Matière d'Expérimentation Animale de Strasbourg (CREMEAS).
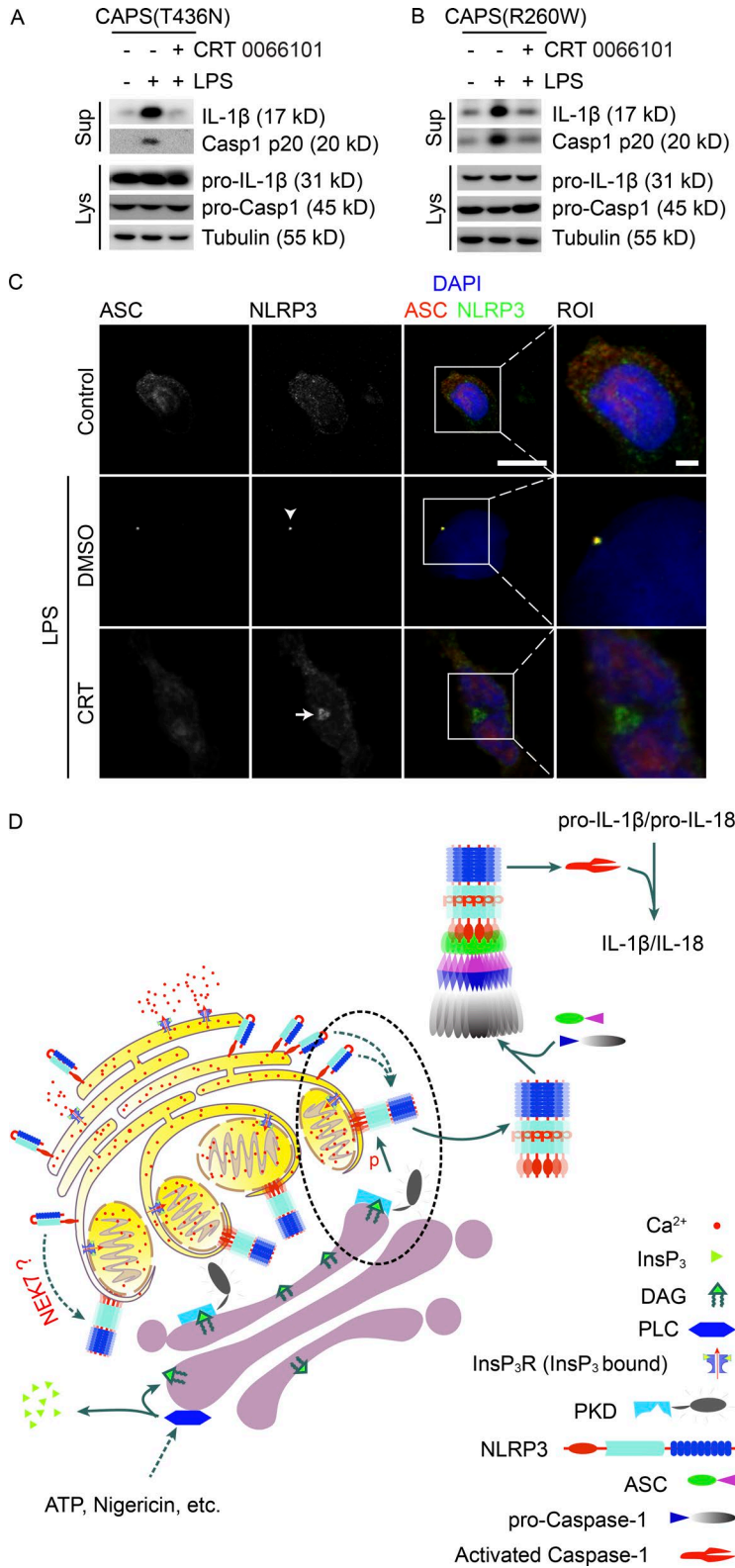
Figure 10. **PKD activity is required for activation of the NLRP3 inflammasome in cells from CAPS patients.** (A and B) Immunoblotting of culture supernatants (Sup) and lysates (Lys) from PBMCs isolated from CAPS patients carrying the *NLRP3* T436N mutation (A) or the R260W mutation (B). Cells were left untreated or treated with 1 µg/ml LPS in the presence of DMSO or CRT 0066101 10 µM for 4 h. (C) Confocal fluorescence imaging of PBMCs isolated from CAPS patients carrying the *NLRP3* T436N mutation were left untreated or treated with 1 µg/ml LPS in the presence of DMSO or 10 µM CRT 0066101 for 4 h. Cells were co-immunostained with antibodies against NLRP3 and ASC. Nuclei were stained with DAPI. Regions of interest (ROIs) are indicated by boxes. Bars: 10 µm; (ROI) 2 µm. (D) Model implementing identified mechanisms in the activation of the NLRP3 inflammasome. The dashed black ellipse highlights the interaction of the Golgi with the MAM. Data shown in A to C are representative of experiments using PBMCs isolated from two CAPS patients carrying the same mutation.

No exclusion of animals used for experiments was performed. Healthy mouse littermates were chosen randomly according to their genotypes.

Reagents

Nigericin sodium salt (catalog no. N7143), BFA (B7651), ATP (A2383), and LPS from *E. coli 055:B5* (L2880) were purchased from Sigma-Aldrich. CRT 0066101 (4975), kb ND 142–70 (3962), 2-APB (1124), BAPTA-AM (2787), U73122 (1268), CID 755673 (3327), Gö 6976 (2253), and Gö 6983 (2285) were purchased from Tocris Bioscience. Nano-SiO₂ (tlrl-sio) and flagellin from *Salmonella typhimurium* (tlrl-stfla) were obtained from InvivoGen. Alum (77161) was purchased from Thermo Fisher Scientific.

Plasmids

Mouse *NLRP3* was amplified from cDNA by PCR. *NLRP3 wt* and *NLRP3* mutants were cloned into pBOB, pLV, or pEGFP-N1 empty vectors using ligation-independent cloning (LIC). Rat *PKCδ C2* (DAG-binding domain), which was amplified from GFP-C1(2) delta (plasmid #21216; Addgene), human *PKD1 wt*, and *PKD1 ΔCRD* were cloned to pBOB empty vector expressing C-terminal–fused EGFP tag. Golgi-localized PKD1 WT, constitutively active, and kinase-dead were cloned by a C-terminal fusion of GRIP domain of p230 as described previously (Kjer-Nielsen et al., 1999). The pX330-P2A-EGFP plasmid was generated by inserting P2A-EGFP sequence into EcoRI-digested pX330-U6-Chimeric_BB-CBh-hSpCas9 (plasmid #42230, Addgene) before stop codon using LIC. Guide RNA (gRNA) sequences were inserted into BbsI-digested pX330-P2A-EGFP plasmid through ligation by T4 DNA ligase.

Cell culture

All mammalian cells were cultured at 37°C, 5% CO₂. Cell lines used in this study are not listed in these databases of commonly misidentified cell lines maintained by ICLAC. THP-1 cells (ATCC) were grown in RPMI 1640 containing 10% fetal bovine serum, 10 mM Hepes, 2.5 g/l glucose, 1 mM sodium pyruvate and gentamycin. HEK293t cells (DKFZ Heidelberg) were grown in DMEM containing 1 g/ml glucose, 10% fetal bovine serum, penicillin and streptomycin. THP-1 cells and HEK293t cells have been authenticated using short tandem repeat performed by LGC Standards. BMDMs were obtained by differentiating bone marrow progenitors from the tibia and femur in RPMI 1640 containing 30% L929-conditional medium or 50 ng/ml recombinant hM-CSF (11343113; Immunotools), 20% heat-inactivated fetal bovine serum, penicillin and streptomycin for 7 d. Peritoneal macrophages were isolated from mice by peritoneal lavage on day 4 after the injection of 3.7% thioglycollate medium (1 ml/mouse). Both BMDMs and peritoneal macrophages were seeded 1 d before experiments using RPMI 1640 containing 10% heat-inactivated fetal bovine serum, penicillin and streptomycin. Human bloods from healthy control and CAPS patients (approved by

the Institut National de la Santé et de la Recherche Médicale ethics committee) were collected after the patients gave their signed informed consent. PBMCs were isolated using Ficoll-Paque PLUS (GE Healthcare) and cultured in RPMI 1640 containing 10% heat-inactivated fetal bovine serum and penicillin and streptomycin. Cell cultures were negative for mycoplasma contamination.

To activate the NLRP3 inflammasome, BMDMs, peritoneal macrophages, or PBMCs were primed with 1 µg/ml LPS for 4 h, followed by the treatment of 2.5 mM or 5 mM ATP for 20 to 40 min, 7.5 µM or 15 µM nigericin for 20 to 40 min, 250 µg/ml or 500 µg/ml alum for 6 h, or 30 to 120 µg/ml nano-SiO₂ for 6 h, whereas THP-1 cells were differentiated by 100 nM PMA treatment for 3 h, followed by overnight incubation with fresh medium before the treatment of NLRP3 inflammasome activators. For the infection of BMDMs by *E. coli* DH5α and *S. aureus* (strain Xen 8.1; Xenogen), overnight cultures of bacteria were seeded in LB medium by 1/100 dilution and grew until OD600 reached 0.6 at 37°C; bacteria were collected by centrifugation and washed three times with sterile 1×PBS. LPS-primed BMDMs were infected at multiplicity of infection of 20 or 50 for 3 h. For activation of AIM2- or NLRC4 inflammasome, LPS-primed BMDMs were transfected with 1 µg/ml poly(dA:dT) or 0.5 µg/ml flagellin, respectively, for 4 h using Lipofectamine 2000 (Life Technology) according to the manufacturer's protocol, whereas for activation of PYRIN inflammasome, LPS-primed BMDMs were treated with 0.1 nM recombinant cytotoxin TcdB for 2 h. For inhibitors treatment, the cells were pretreated with inhibitors for 1 h before the treatment of cognate stimuli in present of inhibitors.

For the packaging of lentivirus, 12 µg Lenti-mix (3 µg pVSVG, 3 µg pMDL, and 3 µg pREV) plus 12 µg of gene of interest expressing plasmid were transfected into HEK293t cells (10-cm plate) using Lipofectamine 2000. After 48 h, the supernatants were collected and filtered using 0.45-µm Millex-HV syringe filters and kept at −80°C. BMDMs and THP-1 cells were infected in fresh medium containing 1 µg/ml polybrene (sc-134220; Santa Cruz) and 25% lentivirus-contained supernatant.

For the knockdown of *PKD2*, 1.0×10^6 BMDMs were seed in each well of a six-well plate on the day before transfection. Cells were transfected with 100 pmol ON-TARGET plus Non-targeting Pool (D-001810-10-05; Dharmacon) or ON-TARGET plus Mouse *PKD2* (101540) siRNA-SMART pool (L-040693-00-0005; Dharmacon) using DharmaFECT 4 Transfection Reagent (T-2004-01; Dharmacon). 36 h after transfection, cells were collected for RNA isolation or treated with LPS plus ATP or nigericin for 40 min to activate the NLRP3 inflammasome.

Gene disruption using CRISPR/Cas9 genome editing system

For generation of *NLRP3* KO THP-1 cell lines, guide RNA (gRNA) sequence (5′-GTACCTGGCCAGCTTGCAGC3′) was cloned into pX330-P2A-EGFP through ligation using

T4 ligase. THP-1 cells were transfected using Cell Line Nucleofector kit V (VCA-1003; Lonza). 24 h after transfection, GFP-positive cells were enriched by FACS (BD FACS Aria II) and seeded into 96-well plates. Obtained *NLRP3*-KO single-cell clones were validated by immunoblotting and sequencing of PCR-amplified targeted fragment. The following primers were used for PCR amplification: 5′-AAA GACTCATCCGTGTGCCGTGTTC-3′ and 5′-TCCCCA TTGAAGTCGATCATTAGCG-3′. Raw264.7-ASC (Raw-ASC) WT, *NLRP3*-KO, *Caspase-1*–KO, and *GSDMD*-KO cell lines were generated as described previously (He et al., 2015). For the generation of *PKD1/2/3* triple KO Raw-ASC cell line, three gRNAs respectively targeting *PKD1* (gRNA sequence: 5′-CTCATGGATGACATGGACG-3′), *PKD2* (gRNA sequence: 5′-TACATCCCCCTGATGCGCG-3′) and *PKD3* (gRNA sequence: 5′-GACCCGACTGATCTC GACG-3′) were used. Obtained *PKD1/PKD2/PKD3* triple-KO single-cell clones were validated by sequencing of PCR-amplified targeted fragments. The following primers were used for PCR amplification: 5′-AGAGAATTCGGA TCCCTGGTTCTAAGAGTCCGGGCT-3′ and 5′-CTT CCATGGCTCGAGCTCTGGGGCAACCAAGCTCC-3′ for PKD1; 5′-AGAGAATTCGGATCCGTGCGTGTG CTCCATATTCACA-3′ and 5′-CTTCCATGGCTCGAG CTTATGGGTCCATGCCAACTCA-3′ for PKD2; 5′-AG AGAATTCGGATCCGACTGGTCTGCTTAGGTGCA TT-3′ and 5′-CTTCCATGGCTCGAGCCTGAATGGAG CTCCTGACCTG-3′ for PKD3.

Measurement of mitochondrial oxygen consumption

OCRs were measured using an XF96 Extracellular Flux Analyzer (Seahorse Bioscience). Measurements were performed using assay medium (Seahorse XF base medium supplemented with 1 mM sodium pyruvate, 2 mM L-glutamine, and 10 mM glucose) according to the Seahorse XF Cell Mito Stress Test kit (part 103015–100; Seahorse Bioscience) user guide. 1.0×10^5 THP-1 WT or NLRP3-defiecnt cells were seed in each well in presence of 100 nM PMA. 3 h later, medium was replaced by fresh medium. The next day, cells were washed once with assay medium and equilibrated with assay medium containing DMSO or 10 µM CRT 0066101 at 37°C for 1 h in an incubator without CO_2. 15 µM nigericin, 2.0 µM oligomycin, 1.0 µM FCCP, and 0.5 µM rotenone/antimycin were sequentially injected at 9 min, 42 min, 60 min, and 78 min. Mixing, waiting, and measurement times were 3, 0, and 3 min, respectively.

Immunoprecipitation and immunoblotting

After treatments, cell supernatants and cell lysates were collected for immunoblotting analysis. Cell lysates were collected in 1× SDS sample buffer or in 1× RIPA buffer (50 mM Tris-HCl, pH 7.5, 150 mM NaCl, 1% Triton X-100, 1 mM EDTA, 1 mM EGTA, 2 mM sodium pyrophosphate, 1 mM NaVO$_4$, and 1 mM NaF) supplemented with protease inhibitor cocktail. The immunoblot were prepared using Tris-glycine SDS-PAGE. For the supernatants, the proteins were extracted using methanol-chloroform precipitation, separated by Tricine SDS-PAGE, and analyzed by immunoblotting. For immunoprecipitation, FLAG-tagged NLRP3 was immunoprecipitated using anti-FLAG M2 Affinity Gel (A2220; Sigma-Aldrich), whereas HA-tagged PKD1 was done using EZview Red Anti-HA Affinity Gel (E6779; Sigma-Aldrich). After washing, bound proteins were eluted by 2× SDS sample buffer and analyzed by immunoblots for NLRP3 or PKD1 with anti-FLAG or anti-HA antibodies. For analysis of the ASC pyroptosome, pellets from whole-cell lysates were cross-linked with disuccinimidyl suberate and analyzed by immunoblotting. The immunoblots were probed overnight at 4°C or 1 h at room temperature with anti–human IL-1β antibody (AF-201-NA; R&D Systems), anti–human caspase-1 antibody (06-503; Merck Millipore), anti–mouse IL-1β antibody (5129-100; BioVision), anti–mouse caspase-1 p10 antibody (sc-514; Santa Cruz Biotechnology), anti–mouse caspase-1 p20 (AG-20B-0042-C100; AdipoGen), anti-ASC antibody (sc-22514; Santa Cruz Biotechnology), anti-NLRP3 antibody (G-20B-0014-C100; AdipoGen); anti-GAPDH (G9545; Sigma-Aldrich), anti-tubulin (T9026; Sigma-Aldrich), anti–phospho-PKD/PKCµ (Ser916) antibody (2051; Cell Signaling Technology), anti–phospho-(Ser/Thr) PKD substrate antibody (4381; Cell Signaling Technology), rabbit anti–phospho-NLRP3 (Ser295) antibody (homemade: serine-phosphorylated "RKP**S**RIL FLC" peptide was used for immunization of rabbits; after the purification using serine-phosphorylated peptide, phosphorylation-specific antibody was obtained through depletion using nonphosphorylated peptide), anti-PKD3 antibody (5655; Cell Signaling Technology), anti-PKD antibody (C-20; sc-639; Santa Cruz Biotechnology), anti-GSDMD (20770–1-AP; Proteintech), anti-GM130 antibody (11308-AP; Proteintech), anti-calnexin antibody (10427-2-AP; Proteintech), anti-Tom20 antibody (sc-11415; Santa Cruz Biotechnology), anti-FLAG antibody (F1804; Sigma-Aldrich); and anti-HA antibody (sc-805; Santa Cruz Biotechnology).

Immunofluorescence microscopy

After treatments, cells plated on coverslips (9–15 mm) were fixed in 4% paraformaldehyde for 15 min at room temperature. Cells were permeabilized for 10 min using 0.25% Triton X-100 in PBS. After blocking with 10% normal goat serum for 1 h, cells were incubated with anti-ASC antibody (1:100 dilution; sc-22514; Santa Cruz Biotechnology), anti-NLRP3 antibody (1:100 dilution; G-20B-0014-C100; AdipoGen; previously approved for immunostaining; Man et al., 2014), anti–phospho-NLRP3 (Ser295) antibody (generated as described in the methodology section Immunoprecipitaion and immunoblotting above; 1:50), anti-giantin antibody (1:300 dilution; ALX-804-600-C100; Enzo Life Science), anti-giantin antibody (1:300 dilution; AB24586; Abcam), anti-GM130 antibody (1:300 dilution; 11308-AP; Proteintech), and anti-Tom20 antibody (1:500 dilution; sc-11415; Santa Cruz

Biotechnology) for 1 h at room temperature. After incubation with secondary antibodies for 1 h at room temperature, cells were stained with DAPI and mounted. Images were acquired using Confocal Laser Scanning Microscope TCS SP8 (Leica).

Cellular fractionation

Isolation of MAMs was performed as described previously (Wieckowski et al., 2009). In brief, $\sim3 \times 10^8$ cells were homogenized using a 15-ml Dounce tissue grinder in buffer containing 30 mM Tris-HCl, pH 7.4, 225 mM mannitol, 75 mM sucrose, and 0.1 mM EGTA. Homogenized cells were centrifuged at 600 g for 5 min to remove nuclei and intact cells. Crude mitochondria pellet was collected by centrifugation at 7,000 g for 10 min. Crude mitochondria pellet was suspended in ice-cold buffer containing 5 mM Hepes-KOH, pH 7.4, 250 mM mannitol, and 0.5 mM EGTA, and layered on top of 8 ml Percoll medium (20%). Pure mitochondria and MAM fractions were separated by centrifugation at 95,000 g for 30 min. Golgi was isolated using Golgi isolation kit (GL0010; Sigma-Aldrich) according to the manufacturer's protocol.

Gel filtration assay

For each condition, cells were plated on ten 150-mm dishes, treated with 100 nM PMA for 3 h, and incubated overnight in fresh medium. The next day, cell were pretreated with DMSO or 10 µM CRT 0066101 for 1 h, followed by treatment with 15 µM nigericin in presence of DMSO or 10 µM CRT 0066101 for 30 min. After the treatments, cells were collected in PBS. Cells were washed twice with ice-cold PBS and sonicated for 2 min (2 s on and 2 s off) on ice in 1× PBS containing 2 mM DTT. Cell lysates were clarified by centrifugation, followed by filtration with 0.2 µm Minisart filter (Sartorius Stedim Biotech). The flow through was injected into Superose 6 Column (GE Healthcare) running at a flow rate of 0.5 ml/min. Fractions were collected by 500 µl for each and analyzed by immunoblotting.

Blue native PAGE

Blue native PAGE electrophoresis was performed using Novex NativePAGE Bis-Tris gel system (Thermo Fisher Scientific). In brief, 2.0×10^6 THP-1 cells after treatments were washed once with ice-cold 1× PBS and then lysed in ice-cold 1× native lysis buffer containing 1% digitonin and EDTA-free protease inhibitor cocktail (Roche Diagnostics) for 30 min on ice. Lysates were clarified by centrifugation at 20,000 g for 30 min at 4°C before quantification using Bradford protein assay (Bio-Rad). Mature inflammasomes were pelleted by centrifugation because of their insolubility. Equal amount of lysates were separated by 3–12% blue native PAGE. Proteins in native gels were transferred to PVDF membranes (Millipore), followed by conventional immunoblotting.

Shotgun mass spectrometry

FLAG-tagged NLRP3 (mouse) was coexpressed with GFP or GFP-tagged constitutively active PKD1 in HEK293t cells.

36 h after transfection, cells were lysed in RIPA buffer. FLAG-tagged NLRP3 was immunoprecipitated using anti-FLAG M2 Affinity Gel. Immunoprecipitated samples were separated by 8% SDS-PAGE gel (14 cm wide × 9 cm long) and stained with Coomassie blue. The bands covering NLRP3 were cut and proceeded for in-gel digestion (Shevchenko et al., 2006) using Asp-N enzyme (Roche Diagnostics). Samples after Asp-N digestion were subjected to LC-MS/MS analysis by Oribtrap XL. The raw files acquired were processed with MaxQuant software (version 1.5.2.8) according to the standard workflow. Database search was performed in MaxQuant with Andromeda search engine against the mouse Swiss-Prot database. The identified results together with the raw data were further visualized by Viewer in MaxQuant and analyzed by Sklyine software.

Flow cytometry

Tibia bones and spleens were isolated from *PKD1-PKD3*^{fl/fl} and *PKD1-PKD3*^{Δmy} mice. Bone marrow cells were flushed out and spleens were homogenized with 1× PBS containing 1% BSA. 2×10^5 cells were used and blocked with antibody against CD32/16 (553141; BD Biosciences) for 5 min at room temperature, followed by staining with antibodies against CD11b (101225; BioLegend), CD11c (561045; BD PharMingen), CD115 (135505; BioLegend), Ly6c (128015; BioLegend), CD117 (105813; BioLegend), CX3CR1 (149009; BioLegend) for 20 min on ice in the dark. After washing, cells were analyzed by FACS (LSRII; BD). Dead cells were excluded by DAPI staining. Monocytes and macrophages were identified as CD11b$^+$CD11c$^-$Ly-6c$^+$CD115$^+$ using FlowJo. Bone marrow derived monocyte/DC progenitors were identified as CD11b$^-$CD11c$^-$CD115$^+$CD117$^+$Cx3CR1$^+$. Counts of monocytes and macrophages were shown as percentage of counted intact cells.

Quantitative PCR

RNA was extracted using TRIzol reagent (Sigma-Aldrich). Complementary DNA was synthesized with Oligo-dT primer using SuperScript II First-Strand cDNA Synthesis kit (Invitrogen) according to the manufacturer's protocol. Quantitative PCR was performed using SYBR Green (Roche Diagnostics) on the LightCycler 480 (Roche Diagnostics). The samples were individually normalized to the housekeeping gene hypoxanthine-guanine phosphoribosyltransferase (*HPRT*). The following primers were used: *Hprt* forward: 5′-TCAGTCAACGGGGGACATAAA-3′, reverse: 5′-GGGGCTGTACTGCTTAACCAG-3′; *TNF* forward: 5′-CATCTTCTCAAAATTCGAGTGACAA-3′, reverse: 5′-TGGGAGTAGACAAGGTACAACCC-3′; *IL-1β* forward: 5′-GCCCATCCTCTGTGACTCAT-3′, reverse: 5′-AGGCCACAGGTATTTTGTCG-3′; *IL-6* forward: 5′-GAGGATACCACTCCCAACAGACC-3′, reverse: 5′-AAGTGCATCATCGTTGTTCATACA-3′; *IL-12p40* forward: 5′-CCTGAAGTGTGAAGCACCAA-3′, reverse: 5′-AGTCCCTTTGGTCCAGTGTG-3′; and *PKD2* for-

ward: 5′-TGTGTTTTCCTCCATAAACC-3′, reverse: 5′-CCACTGTCTACCAGATCTTC-3′.

LPS injection and peritoneal infection of *S. aureus* in mice

LPS were injected into mice at a dose of 20 mg/kg. Blood was collected at 2 h after injection. For *S. aureus* infection, bacteria cultures in exponential growth phase were centrifuged and the pellet was resuspended in 1× PBS. Approximately 7×10^8 CFUs of luminescent *S. aureus* in 200 µl were inoculated to each anesthetized mouse by peritoneal injection. Hairs were removed by chemical depilation before inoculation. Body temperature were measured at 6 h after inoculation. Luminescence was monitored immediately after the inoculation and at 6 h after inoculation with a CCD camera using an IVIS50 system from Caliper (5 min exposure of the animals), and quantification was done with the Living Image3.2 program from Xenogen/Caliper. For inhibitor pretreatment, 10 mg/kg CRT 0066101 was injected at 1 h before LPS injection or *S. aureus* inoculation.

Measurement of cytokines using ELISA

Mouse IL-1β, TNF, and IL-6 in cell culture supernatants were measured using the MILLIPLE MAP mouse cytokines multiplex assay according to the manufacturer's protocol. Human IL-1β was measured using the Quantikine ELISA Human IL-1/IL1F2 Immunoassay (DLB50; R&D Systems). Mouse serum IL-1β was measured using the Quantikine ELISA mouse IL-1/IL1F2 Immunoassay (MLB00C; R&D Systems).

Statistical analyses

Preliminary experiments were performed and sample size was determined based on generally accepted rules to test preliminary conclusions reaching statistical significance, where applicable. Gehan–Breslow–Wilcoxon tests were performed for survival curves; Mann–Whitney tests were performed for serum IL-1β levels, body temperatures, and bacterial loads. Statistical analyses for the other experiments were performed with the *t* test using Prism (GraphPad Software).

Online supplemental material

Fig. S1 includes additional data related to Fig. 4, showing that deficiency of PKD blocks the activation of NLRP3 inflammasome without affecting lineage development of mouse myeloid cells, LPS priming and secretion of other NF-κB–dependent cytokines. Fig. S2 includes additional data related to Figs. 6 and 7, showing that the requirement of PKD activity is specific for NLRP3 inflammasome, but not the other inflammasomes. Fig. S3 shows PKD acts downstream of mitochondrial clustering and dysfunction. Fig. S4 includes additional data related to Fig. 8, consolidating the phosphorylation of NLRP3 at Ser 293 by PKD. Fig. S5 shows that PKD acts downstream of self-oligomerization of NLRP3.

REFERENCES

Abe, K., H. Fuchs, A. Boersma, W. Hans, P. Yu, S. Kalaydjiev, M. Klaften, T. Adler, J. Calzada-Wack, I. Mossbrugger, et al. 2011. A novel N-ethyl-N-nitrosourea-induced mutation in phospholipase Cγ2 causes inflammatory arthritis, metabolic defects, and male infertility in vitro in a murine model. *Arthritis Rheum.* 63:1301–1311. http://dx.doi.org/10.1002/art.30280

Agostini, L., F. Martinon, K. Burns, M.F. McDermott, P.N. Hawkins, and J. Tschopp. 2004. NALP3 forms an IL-1β–processing inflammasome with increased activity in Muckle–Wells autoinflammatory disorder. *Immunity.* 20:319–325. http://dx.doi.org/10.1016/S1074-7613(04)00046-9

Aksentijevich, I., C.D. Putnam, E.F. Remmers, J.L. Mueller, J. Le, R.D. Kolodner, Z. Moak, M. Chuang, F. Austin, R. Goldbach-Mansky, et al. 2007. The clinical continuum of cryopyrinopathies: Novel CIAS1 mutations in North American patients and a new cryopyrin model. *Arthritis Rheum.* 56:1273–1285. http://dx.doi.org/10.1002/art.22491

Barker, S.A., K.K. Caldwell, J.R. Pfeiffer, and B.S. Wilson. 1998. Wortmannin-sensitive phosphorylation, translocation, and activation of PLCγ1, but not PLCγ2, in antigen-stimulated RBL-2H3 mast cells. *Mol. Biol. Cell.* 9:483–496. http://dx.doi.org/10.1091/mbc.9.2.483

Baroja-Mazo, A., F. Martín-Sánchez, A.I. Gomez, C.M. Martínez, J. Amores-Iniesta, V. Compan, M. Barberà-Cremades, J. Yagüe, E. Ruiz-Ortiz, J. Antón, et al. 2014. The NLRP3 inflammasome is released as a particulate danger signal that amplifies the inflammatory response. *Nat. Immunol.* 15:738–748. http://dx.doi.org/10.1038/ni.2919

Baron, C.L., and V. Malhotra. 2002. Role of diacylglycerol in PKD recruitment to the TGN and protein transport to the plasma membrane. *Science.* 295:325–328. http://dx.doi.org/10.1126/science.1066759

Broz, P., and V.M. Dixit. 2016. Inflammasomes: Mechanism of assembly, regulation and signalling. *Nat. Rev. Immunol.* 16:407–420. http://dx.doi.org/10.1038/nri.2016.58

Brydges, S.D., J.L. Mueller, M.D. McGeough, C.A. Pena, A. Misaghi, C. Gandhi, C.D. Putnam, D.L. Boyle, G.S. Firestein, A.A. Horner, et al. 2009. Inflammasome-mediated disease animal models reveal roles for innate but not adaptive immunity. *Immunity.* 30:875–887. http://dx.doi.org/10.1016/j.immuni.2009.05.005

Chae, J.J., Y.H. Park, C. Park, I.-Y. Hwang, P. Hoffmann, J.H. Kehrl, I. Aksentijevich, and D.L. Kastner. 2015. Connecting two pathways through Ca²⁺ signaling: NLRP3 inflammasome activation induced by a hypermorphic PLCG2 mutation. *Arthritis Rheumatol.* 67:563–567. http://dx.doi.org/10.1002/art.38961

Chuang, Y.-T., Y.-C. Lin, K.-H. Lin, T.-F. Chou, W.-C. Kuo, K.-T. Yang, P.-R. Wu, R.-H. Chen, A. Kimchi, and M.-Z. Lai. 2011. Tumor suppressor death-associated protein kinase is required for full IL-1β production. *Blood.* 117:960–970. http://dx.doi.org/10.1182/blood-2010-08-303115

Codazzi, F., M.N. Teruel, and T. Meyer. 2001. Control of astrocyte Ca²⁺ oscillations and waves by oscillating translocation and activation of protein kinase C. *Curr. Biol.* 11:1089–1097. http://dx.doi.org/10.1016/S0960-9822(01)00326-8

Dowds, T.A., J. Masumoto, F.F. Chen, Y. Ogura, N. Inohara, and G. Núñez. 2003. Regulation of cryopyrin/Pypaf1 signaling by pyrin, the familial Mediterranean fever gene product. *Biochem. Biophys. Res. Commun.* 302:575–580. http://dx.doi.org/10.1016/S0006-291X(03)00221-3

Everett, K.L., T.D. Bunney, Y. Yoon, F. Rodrigues-Lima, R. Harris, P.C. Driscoll, K. Abe, H. Fuchs, M.H. de Angelis, P. Yu, et al. 2009. Characterization of phospholipase C γ enzymes with gain-of-function mutations. *J. Biol. Chem.* 284:23083–23093. http://dx.doi.org/10.1074/jbc.M109.019265

Fielitz, J., M.-S. Kim, J.M. Shelton, X. Qi, J.A. Hill, J.A. Richardson, R. Bassel-Duby, and E.N. Olson. 2008. Requirement of protein kinase D1 for pathological cardiac remodeling. *Proc. Natl. Acad. Sci. USA.* 105:3059–3063. http://dx.doi.org/10.1073/pnas.0712265105

Gross, O., H. Poeck, M. Bscheider, C. Dostert, N. Hannesschläger, S. Endres, G. Hartmann, A. Tardivel, E. Schweighoffer, V. Tybulewicz, et al. 2009. Syk kinase signalling couples to the Nlrp3 inflammasome for anti-fungal host defence. *Nature.* 459:433–436. http://dx.doi.org/10.1038/nature07965

Guo, C., S. Xie, Z. Chi, J. Zhang, Y. Liu, L. Zhang, M. Zheng, X. Zhang, D. Xia, Y. Ke, et al. 2016. Bile acids control inflammation and metabolic disorder through inhibition of NLRP3 inflammasome. *Immunity.* 45:802–816. (published erratum appears in *Immunity.* 2016. http://dx.doi.org/10.1016/j.immuni.2016.10.009) http://dx.doi.org/10.1016/j.immuni.2016.09.008

Gurung, P., J.R. Lukens, and T.-D. Kanneganti. 2015. Mitochondria: Diversity in the regulation of the NLRP3 inflammasome. *Trends Mol. Med.* 21:193–201. http://dx.doi.org/10.1016/j.molmed.2014.11.008

He, W.T., H. Wan, L. Hu, P. Chen, X. Wang, Z. Huang, Z.-H. Yang, C.-Q. Zhong, and J. Han. 2015. Gasdermin D is an executor of pyroptosis and required for interleukin-1β secretion. *Cell Res.* 25:1285–1298. http://dx.doi.org/10.1038/cr.2015.139

He, Y., M.Y. Zeng, D. Yang, B. Motro, and G. Núñez. 2016. NEK7 is an essential mediator of NLRP3 activation downstream of potassium efflux. *Nature.* 530:354–357. http://dx.doi.org/10.1038/nature16959

Horng, T. 2014. Calcium signaling and mitochondrial destabilization in the triggering of the NLRP3 inflammasome. *Trends Immunol.* 35:253–261. http://dx.doi.org/10.1016/j.it.2014.02.007

Ito, M., T. Shichita, M. Okada, R. Komine, Y. Noguchi, A. Yoshimura, and R. Morita. 2015. Bruton's tyrosine kinase is essential for NLRP3

inflammasome activation and contributes to ischaemic brain injury. *Nat. Commun.* 6:7360. http://dx.doi.org/10.1038/ncomms8360

Iyer, S.S., Q. He, J.R. Janczy, E.I. Elliott, Z. Zhong, A.K. Olivier, J.J. Sadler, V. Knepper-Adrian, R. Han, L. Qiao, et al. 2013. Mitochondrial cardiolipin is required for Nlrp3 inflammasome activation. *Immunity.* 39:311–323. http://dx.doi.org/10.1016/j.immuni.2013.08.001

Jin, T.G., T. Satoh, Y. Liao, C. Song, X. Gao, K. Kariya, C.D. Hu, and T. Kataoka. 2001. Role of the CDC25 homology domain of phospholipase Cε in amplification of Rap1-dependent signaling. *J. Biol. Chem.* 276:30301–30307. http://dx.doi.org/10.1074/jbc.M103530200

Jo, E.-K., J.K. Kim, D.-M. Shin, and C. Sasakawa. 2016. Molecular mechanisms regulating NLRP3 inflammasome activation. *Cell. Mol. Immunol.* 13:148–159. http://dx.doi.org/10.1038/cmi.2015.95

Katsnelson, M.A., L.G. Rucker, H.M. Russo, and G.R. Dubyak. 2015. K⁺ efflux agonists induce NLRP3 inflammasome activation independently of Ca²⁺ signaling. *J. Immunol.* 194:3937–3952. http://dx.doi.org/10.4049/jimmunol.1402658

Kayagaki, N., I.B. Stowe, B.L. Lee, K. O'Rourke, K. Anderson, S. Warming, T. Cuellar, B. Haley, M. Roose-Girma, Q.T. Phung, et al. 2015. Caspase-11 cleaves gasdermin D for non-canonical inflammasome signalling. *Nature.* 526:666–671. http://dx.doi.org/10.1038/nature15541

Kjer-Nielsen, L., R.D. Teasdale, C. van Vliet, and P.A. Gleeson. 1999. A novel Golgi-localisation domain shared by a class of coiled-coil peripheral membrane proteins. *Curr. Biol.* 9:385–390. http://dx.doi.org/10.1016/S0960-9822(99)80168-7

Koss, H., T.D. Bunney, S. Behjati, and M. Katan. 2014. Dysfunction of phospholipase Cγ in immune disorders and cancer. *Trends Biochem. Sci.* 39:603–611. http://dx.doi.org/10.1016/j.tibs.2014.09.004

Lamkanfi, M., and V.M. Dixit. 2012. Inflammasomes and their roles in health and disease. *Annu. Rev. Cell Dev. Biol.* 28:137–161. http://dx.doi.org/10.1146/annurev-cellbio-101011-155745

Lamkanfi, M., and V.M. Dixit. 2014. Mechanisms and functions of inflammasomes. *Cell.* 157:1013–1022. http://dx.doi.org/10.1016/j.cell.2014.04.007

Latz, E., T.S. Xiao, and A. Stutz. 2013. Activation and regulation of the inflammasomes. *Nat. Rev. Immunol.* 13:397–411. http://dx.doi.org/10.1038/nri3452

Lee, G.-S., N. Subramanian, A.I. Kim, I. Aksentijevich, R. Goldbach-Mansky, D.B. Sacks, R.N. Germain, D.L. Kastner, and J.J. Chae. 2012. The calcium-sensing receptor regulates the NLRP3 inflammasome through Ca²⁺ and cAMP. *Nature.* 492:123–127. http://dx.doi.org/10.1038/nature11588

Liljedahl, M., Y. Maeda, A. Colanzi, I. Ayala, J. Van Lint, and V. Malhotra. 2001. Protein kinase D regulates the fission of cell surface destined transport carriers from the trans-Golgi network. *Cell.* 104:409–420. http://dx.doi.org/10.1016/S0092-8674(01)00228-8

Lu, B., T. Nakamura, K. Inouye, J. Li, Y. Tang, P. Lundbäck, S.I. Valdes-Ferrer, P.S. Olofsson, T. Kalb, J. Roth, et al. 2012. Novel role of PKR in inflammasome activation and HMGB1 release. *Nature.* 488:670–674. http://dx.doi.org/10.1038/nature11290

Man, S.M., L.J. Hopkins, E. Nugent, S. Cox, I.M. Glück, P. Tourlomousis, J.A. Wright, P. Cicuta, T.P. Monie, and C.E. Bryant. 2014. Inflammasome activation causes dual recruitment of NLRC4 and NLRP3 to the same macromolecular complex. *Proc. Natl. Acad. Sci. USA.* 111:7403–7408. http://dx.doi.org/10.1073/pnas.1402911111

Mariathasan, S., D.S. Weiss, K. Newton, J. McBride, K. O'Rourke, M. Roose-Girma, W.P. Lee, Y. Weinrauch, D.M. Monack, and V.M. Dixit. 2006. Cryopyrin activates the inflammasome in response to toxins and ATP. *Nature.* 440:228–232. http://dx.doi.org/10.1038/nature04515

Martin, B.N., C. Wang, J. Willette-Brown, T. Herjan, M.F. Gulen, H. Zhou, K. Bulek, L. Franchi, T. Sato, E.S. Alnemri, et al. 2014. IKKα negatively

regulates ASC-dependent inflammasome activation. *Nat. Commun.* 5:4977. http://dx.doi.org/10.1038/ncomms5977

Martinon, F., L. Agostini, E. Meylan, and J. Tschopp. 2004. Identification of bacterial muramyl dipeptide as activator of the NALP3/cryopyrin inflammasome. *Curr. Biol.* 14:1929–1934. http://dx.doi.org/10.1016/j.cub.2004.10.027

Martinon, F., V. Pétrilli, A. Mayor, A. Tardivel, and J. Tschopp. 2006. Gout-associated uric acid crystals activate the NALP3 inflammasome. *Nature.* 440:237–241. http://dx.doi.org/10.1038/nature04516

Menu, P., A. Mayor, R. Zhou, A. Tardivel, H. Ichijo, K. Mori, and J. Tschopp. 2012. ER stress activates the NLRP3 inflammasome via an UPR-independent pathway. *Cell Death Dis.* 3:e261. http://dx.doi.org/10.1038/cddis.2011.132

Miller, L.S., E.M. Pietras, L.H. Uricchio, K. Hirano, S. Rao, H. Lin, R.M. O'Connell, Y. Iwakura, A.L. Cheung, G. Cheng, and R.L. Modlin. 2007. Inflammasome-mediated production of IL-1β is required for neutrophil recruitment against *Staphylococcus aureus* in vivo. *J. Immunol.* 179:6933–6942. http://dx.doi.org/10.4049/jimmunol.179.10.6933

Mortimer, L., F. Moreau, J.A. MacDonald, and K. Chadee. 2016. NLRP3 inflammasome inhibition is disrupted in a group of auto-inflammatory disease CAPS mutations. *Nat. Immunol.* 17:1176–1186. http://dx.doi.org/10.1038/ni.3538

Muñoz-Planillo, R., P. Kuffa, G. Martínez-Colón, B.L. Smith, T.M. Rajendiran, and G. Núñez. 2013. K⁺ efflux is the common trigger of NLRP3 inflammasome activation by bacterial toxins and particulate matter. *Immunity.* 38:1142–1153. http://dx.doi.org/10.1016/j.immuni.2013.05.016

Murakami, T., J. Ockinger, J. Yu, V. Byles, A. McColl, A.M. Hofer, and T. Horng. 2012. Critical role for calcium mobilization in activation of the NLRP3 inflammasome. *Proc. Natl. Acad. Sci. USA.* 109:11282–11287. http://dx.doi.org/10.1073/pnas.1117765109

Nakahira, K., J.A. Haspel, V.A.K. Rathinam, S.-J. Lee, T. Dolinay, H.C. Lam, J.A. Englert, M. Rabinovitch, M. Cernadas, H.P. Kim, et al. 2011. Autophagy proteins regulate innate immune responses by inhibiting the release of mitochondrial DNA mediated by the NALP3 inflammasome. *Nat. Immunol.* 12:222–230. http://dx.doi.org/10.1038/ni.1980

Nakamura, Y., L. Franchi, N. Kambe, G. Meng, W. Strober, and G. Núñez. 2012. Critical role for mast cells in interleukin-1β-driven skin inflammation associated with an activating mutation in the nlrp3 protein. *Immunity.* 37:85–95. http://dx.doi.org/10.1016/j.immuni.2012.04.013

Ombrello, M.J., E.F. Remmers, G. Sun, A.F. Freeman, S. Datta, P. Torabi-Parizi, N. Subramanian, T.D. Bunney, R.W. Baxendale, M.S. Martins, et al. 2012. Cold urticaria, immunodeficiency, and autoimmunity related to PLCG2 deletions. *N. Engl. J. Med.* 366:330–338. http://dx.doi.org/10.1056/NEJMoa1102140

Pétrilli, V., S. Papin, C. Dostert, A. Mayor, F. Martinon, and J. Tschopp. 2007. Activation of the NALP3 inflammasome is triggered by low intracellular potassium concentration. *Cell Death Differ.* 14:1583–1589. http://dx.doi.org/10.1038/sj.cdd.4402195

Ponpuak, M., M.A. Mandell, T. Kimura, S. Chauhan, C. Cleyrat, and V. Deretic. 2015. Secretory autophagy. *Curr. Opin. Cell Biol.* 35:106–116. http://dx.doi.org/10.1016/j.ceb.2015.04.016

Rathinam, V.A.K., and K.A. Fitzgerald. 2016. Inflammasome complexes: Emerging mechanisms and effector functions. *Cell.* 165:792–800. http://dx.doi.org/10.1016/j.cell.2016.03.046

Rhee, S.G. 2001. Regulation of phosphoinositide-specific phospholipase C. *Annu. Rev. Biochem.* 70:281–312. http://dx.doi.org/10.1146/annurev.biochem.70.1.281

Rossol, M., M. Pierer, N. Raulien, D. Quandt, U. Meusch, K. Rothe, K. Schubert, T. Schöneberg, M. Schaefer, U. Krügel, et al. 2012. Extracellular Ca2+ is a danger signal activating the NLRP3 inflammasome through G protein-coupled calcium sensing receptors. *Nat. Commun.* 3:1329. http://dx.doi.org/10.1038/ncomms2339

Rozengurt, E., O. Rey, and R.T. Waldron. 2005. Protein kinase D signaling. *J. Biol. Chem.* 280:13205–13208. http://dx.doi.org/10.1074/jbc.R500002200

Rubartelli, A., F. Cozzolino, M. Talio, and R. Sitia. 1990. A novel secretory pathway for interleukin-1 β, a protein lacking a signal sequence. *EMBO J.* 9:1503–1510.

Rykx, A., L. De Kimpe, S. Mikhalap, T. Vantus, T. Seufferlein, J.R. Vandenheede, and J. Van Lint. 2003. Protein kinase D: A family affair. *FEBS Lett.* 546:81–86. http://dx.doi.org/10.1016/S0014-5793(03)00487-3

Sander, L.E., M.J. Davis, M.V. Boekschoten, D. Amsen, C.C. Dascher, B. Ryffel, J.A. Swanson, M. Müller, and J.M. Blander. 2011. Detection of prokaryotic mRNA signifies microbial viability and promotes immunity. *Nature.* 474:385–389. http://dx.doi.org/10.1038/nature10072

Schmid-Burgk, J.L., D. Chauhan, T. Schmidt, T.S. Ebert, J. Reinhardt, E. Endl, and V. Hornung. 2016. A genome-wide CRISPR (clustered regularly interspaced short palindromic repeats) screen identifies NEK7 as an essential component of NLRP3 inflammasome activation. *J. Biol. Chem.* 291:103–109. http://dx.doi.org/10.1074/jbc.C115.700492

Schroder, K., and J. Tschopp. 2010. The inflammasomes. *Cell.* 140:821–832. http://dx.doi.org/10.1016/j.cell.2010.01.040

Shevchenko, A., H. Tomas, J. Havlis, J.V. Olsen, and M. Mann. 2006. In-gel digestion for mass spectrometric characterization of proteins and proteomes. *Nat. Protoc.* 1:2856–2860. http://dx.doi.org/10.1038/nprot.2006.468

Shi, H., Y. Wang, X. Li, X. Zhan, M. Tang, M. Fina, L. Su, D. Pratt, C.H. Bu, S. Hildebrand, et al. 2016. NLRP3 activation and mitosis are mutually exclusive events coordinated by NEK7, a new inflammasome component. *Nat. Immunol.* 17:250–258. http://dx.doi.org/10.1038/ni.3333

Shi, J., Y. Zhao, K. Wang, X. Shi, Y. Wang, H. Huang, Y. Zhuang, T. Cai, F. Wang, and F. Shao. 2015. Cleavage of GSDMD by inflammatory caspases determines pyroptotic cell death. *Nature.* 526:660–665. http://dx.doi.org/10.1038/nature15514

Shimada, K., T.R. Crother, J. Karlin, J. Dagvadorj, N. Chiba, S. Chen, V.K. Ramanujan, A.J. Wolf, L. Vergnes, D.M. Ojcius, et al. 2012. Oxidized mitochondrial DNA activates the NLRP3 inflammasome during apoptosis. *Immunity.* 36:401–414. http://dx.doi.org/10.1016/j.immuni.2012.01.009

Storz, P., H. Döppler, and A. Toker. 2005. Protein kinase D mediates mitochondrion-to-nucleus signaling and detoxification from mitochondrial reactive oxygen species. *Mol. Cell. Biol.* 25:8520–8530. http://dx.doi.org/10.1128/MCB.25.19.8520-8530.2005

Strowig, T., J. Henao-Mejia, E. Elinav, and R. Flavell. 2012. Inflammasomes in health and disease. *Nature.* 481:278–286. http://dx.doi.org/10.1038/nature10759

Stutz, A., C.-C. Kolbe, R. Stahl, G.L. Horvath, B.S. Franklin, O. van Ray, R. Brinkschulte, M. Geyer, F. Meissner, and E. Latz. 2017. NLRP3 inflammasome assembly is regulated by phosphorylation of the pyrin domain. *J. Exp. Med.* 214:1725–1736. http://dx.doi.org/10.1084/jem.20160933

Subramanian, N., K. Natarajan, M.R. Clatworthy, Z. Wang, and R.N. Germain. 2013. The adaptor MAVS promotes NLRP3 mitochondrial localization and inflammasome activation. *Cell.* 153:348–361. http://dx.doi.org/10.1016/j.cell.2013.02.054

Uesugi, A., A. Kataoka, H. Tozaki-Saitoh, Y. Koga, M. Tsuda, B. Robaye, J.-M. Boeynaems, and K. Inoue. 2012. Involvement of protein kinase D in uridine diphosphate-induced microglial macropinocytosis and phagocytosis. *Glia.* 60:1094–1105. http://dx.doi.org/10.1002/glia.22337

Wang, X., W. Jiang, Y. Yan, T. Gong, J. Han, Z. Tian, and R. Zhou. 2014. RNA viruses promote activation of the NLRP3 inflammasome through a

2692

Protein kinase D activates the NLRP3 inflammasome | Zhang et al.

RIP1–RIP3–DRP1 signaling pathway. *Nat. Immunol.* 15:1126–1133. http://dx.doi.org/10.1038/ni.3015

Wieckowski, M.R., C. Giorgi, M. Lebiedzinska, J. Duszynski, and P. Pinton. 2009. Isolation of mitochondria-associated membranes and mitochondria from animal tissues and cells. *Nat. Protoc.* 4:1582–1590. http://dx.doi.org/10.1038/nprot.2009.151

Yang, C.-S., J.-J. Kim, T.S. Kim, P.Y. Lee, S.Y. Kim, H.-M. Lee, D.-M. Shin, L.T. Nguyen, M.-S. Lee, H.S. Jin, et al. 2015. Small heterodimer partner interacts with NLRP3 and negatively regulates activation of the NLRP3 inflammasome. *Nat. Commun.* 6:6115. http://dx.doi.org/10.1038/ncomms7115

Yu, P., R. Constien, N. Dear, M. Katan, P. Hanke, T.D. Bunney, S. Kunder, L. Quintanilla-Martinez, U. Huffstadt, A. Schröder, et al. 2005. Autoimmunity and inflammation due to a gain-of-function mutation in phospholipase Cγ2 that specifically increases external Ca^{2+} entry. *Immunity.* 22:451–465. http://dx.doi.org/10.1016/j.immuni.2005.01.018

Zhang, T., U. Braun, and M. Leitges. 2016. PKD3 deficiency causes alterations in microtubule dynamics during the cell cycle. *Cell Cycle.* 15:1844–1854. http://dx.doi.org/10.1080/15384101.2016.1188237

Zhou, Q., G.-S. Lee, J. Brady, S. Datta, M. Katan, A. Sheikh, M.S. Martins, T.D. Bunney, B.H. Santich, S. Moir, et al. 2012. A hypermorphic missense mutation in PLCG2, encoding phospholipase Cγ2, causes a dominantly inherited autoinflammatory disease with immunodeficiency. *Am. J. Hum. Genet.* 91:713–720. http://dx.doi.org/10.1016/j.ajhg.2012.08.006

Zhou, R., A.S. Yazdi, P. Menu, and J. Tschopp. 2011. A role for mitochondria in NLRP3 inflammasome activation. *Nature.* 469:221–225. http://dx.doi.org/10.1038/nature09663